Effects of Strain on Activated-Aluminum–Water Reactions

by

Daniel P. Moriarty
B.S., Mechanical Engineering
United States Naval Academy, 2020

Submitted to the Department of Materials Science and Engineering and the Department of Mechanical Engineering in partial fulfillment of the requirements for the degrees of

Master of Science in Materials Science and Engineering
and
Master of Science in Mechanical Engineering
at the
Massachusetts Institute of Technology

September 2022

Author .....
Department of Materials Science and Engineering
Department of Mechanical Engineering
12 August, 2022

Certified by .....
Thomas W. Eagar
Professor of Materials Engineering and Engineering Systems
Thesis Supervisor

Certified by .....
Douglas P. Hart
Professor of Mechanical Engineering
Thesis Reader

Accepted by .....
Frances M. Ross
Ellen Swallow Richards Professor in Materials Science and Engineering
Chair, Departmental Committee on Graduate Studies

Accepted by .....
Nicolas Hadjiconstantinou
Professor of Mechanical Engineering
Chair, Departmental Committee on Graduate Studies

Effects of Strain on Activated-Aluminum–Water Reactions

by

Daniel P. Moriarty

Submitted to the Department of Materials Science and Engineering and the Department of Mechanical Engineering on 12 August, 2022 in Partial Fulfillment of the Requirement of the Degrees of Master of Science in Materials Science and Engineering and Master of Science in Mechanical Engineering

ABSTRACT

Activated aluminum is a fuel source that promises safe hydrogen energy storage with volumetric energy densities twice that of diesel fuel and 45 times that of lithium-ion batteries. Aluminum is activated when liquid eutectic gallium-indium disrupts the aluminum's passive oxide layer, enabling a reaction with water to release hydrogen gas and heat. This thesis seeks further understanding of this reaction by exploring the effect of residual stresses in the aluminum. Annealing and cold rolling of 1100-alloy aluminum plate developed engineering strain levels up to -0.7. Reactions in both DI water and water with 3.5% NaCl salinity and 0.1M caffeine dopant showed no correlation between hydrogen production and strain but an aggressive acceleration of the reaction with increased strain levels. Some reactions produced unreacted aluminum in the product, most notably for high strain level (-0.4 – -0.6) reactions in DI water. The unreacted products, confirmed to be aluminum by SEM-EDS, fully reacted over 24 hours. Using SEM to inspect the first stages of microstructural reaction mechanisms, higher amounts of exfoliated aluminum were expelled from the bulk at high (-0.6) strain levels compared to unstrained (0.0) samples. These observations further understanding of how strain conditions affect activated aluminum reactions and help delineate ideal operating conditions for reactor design.

Thesis Supervisor: Thomas W. Eagar
Title: Professor of Materials Engineering and Engineering Systems

Thesis Reader: Douglas P. Hart
Title: Professor of Mechanical Engineering

Acknowledgements

While this thesis holds only my name on the byline, it was absolutely a community effort to design, develop, edit, and publish it. I owe thanks to many people and this page only begins to express my gratitude to them.

My advisor, Tom Eagar, for helping me restart my degree, find a project, fund my education, and endlessly encouraged me to go after my interests.

Group 47 at Lincoln Lab, especially Eric Morgan and Erik Limpaecher, for their guidance, support, and willingness to invest their time and money, as well as the Technology Office for their sponsorship. Alex and Jonny Slocum, as contractors, were equally willing to aid and troubleshoot from the outside.

Peter Godart and Doug Hart, for their unbounded willingness to share knowledge, wisdom, and funds. Their immediate willingness to guide so much of this project was essential to making this thesis well-developed and finding useful data.

For selflessly providing resources and advice, Antoine Allanore, Charles Boury, Cem Taşan, and Gianluca Roscioli. For acceptance, knowledge, and support over my first year, Cem Taşan, Shaolou Wei, and Allegheny Technologies Inc.

My roommates, Emma, Ava, Lois, and Rory, for keeping me sane.

My family, Mom, Dad, Becca, Theresa, Kim, Kelly, Grandma, and Nana, for their support and love. Many initial drafts and questions of how to proceed passed through all of you, and I could not have done this without your aid.

My friends across MIT and USNA, for your support and energy these past years. Allison, Miranda, Charles, Gavin, Bianca, Kyle, Haley, Jon, Jacob, RJ, Charlotte, Alan, Maya, Rob, Reed, and many others whose small acts of kindness could fill a book.

Contents

List of Figures

List of Abbreviations

Al ..... Aluminum
C ..... Carbon
Ca ..... Calcium
Cl ..... Chlorine
Cu ..... Copper
DI ..... DeIonized
EDS ..... Electron-Dispersive X-ray Spectroscopy
eGaIn ..... Eutectic Gallium-Indium
Fe ..... Iron
Ga ..... Gallium
H ..... Hydrogen
In ..... Indium
K ..... Potassium
Mg ..... Magnesium
MIT ..... Massachusetts Institute of Technology
Mn ..... Manganese
Na ..... Sodium
O ..... Oxygen
Si ..... Silicon
S ..... Sulfur
SEM ..... Scanning Electron Microscope
Zn ..... Zinc

Chapter 1: Background

Aluminum holds great promise as an alternative fuel source. Its volumetric energy density is over twice that of diesel and gasoline. Aluminum's reactions with water and oxygen produce hydrogen gas and a large amount of heat, both of which have well-developed processes for making useful mechanical work. Aluminum scrap is readily available, not only in developed societies, but also in less-developed and disaster regions. A few nanometers of passive oxide are all that prohibit this reaction from freely taking place. Breaking through this oxide has long been the stopping point of aluminum fuel development, as doing so requires passivation from extremely caustic chemicals, dilution to the point of decreased usefulness, or powderization into an extremely reactive compound. Recent passivation using surface treatments of liquid metals at room temperature, typically involving gallium and indium, has enabled the reaction of aluminum and water to take place in chemically safe environments with minimal preparation.

Using eutectic gallium-indium to surface-treat aluminum for reaction in water is a developing method, warranting further research to identify ideal operating conditions for energy-generating applications. Previous researchers have noted how small changes in the reactants can greatly change the efficacy of the reaction.

Residual stress levels in the aluminum appear to affect the reaction completion, while using ionic solutions as opposed to deionized water can change the reaction rate and recoverability of the treatment chemical. Another key motivating data point was that the observation of the reaction at high magnification showed highly delaminated grains, reminiscent of residual stress.

Considering these previous observations, this thesis set out to answer the following questions:

1. What is the effect of strain on the reaction between activated aluminum and water?

2. Does the reaction differ between seawater and DI water?

3. Is microscopic grain delamination an effect of residual stress?

Samples, specially developed to have controlled levels of high strain and treated for minimal effect on residual stresses, were tested for hydrogen production and reaction duration. No correlation between hydrogen production and strain was seen, but an acceleration of the reaction occurred at increasing strain levels. These tests also produced the unexpected phenomenon of unreacted aluminum in cases of high-strain, DI-water reactions and some seawater reactions. The

unreacted aluminum contributed to a large variability in hydrogen production but able to completely react over 24 hours. Using a scanning electron microscope to observe slightly reacted samples, delamination occurred in grains ejected from the sample bulk in sites surrounded by circular patterns. These occurred in both highly strained and unstrained samples, though the quantity of ejected grains was far greater and the scale of the delamination and ejection sites were smaller in highly strained samples. This thesis records the motivation and process used to find these results and presents them, with suggestions for future work, for comprehension of the activated-aluminum–water reaction to benefit design of energy-generating reactors.

1.1 The Search for New Fuel Sources

Society's current consumption rate of fuel sources is not sustainable. A large amount of power comes from burning hydrocarbons, which are produced under colossal levels of pressure and on a geologic timescale. In delving further into the earth in mine after mine for products of coal, natural gas, and gasoline, those reserves are depleted at an astonishing rate. The US Energy Information Administration's International Energy Outlook, 2021, states that fossil fuel reserves are only adequate to meet our demands through 2050 [1]. While new sources of hydrocarbons may yet be discovered, it is likely that this resource will run out in the near future, hence planning for other sources of fuel is necessary for sustaining society.

A more immediate threat than fuel scarcity, however, is that of global warming. As the average temperature of the earth rises from pre-industrial levels (1.19°C since 1900) [2], natural disasters including heatwaves, wildfires, and droughts will become more common with increasing severity. Sea level has risen by 7-8 inches since 1900, with 3 inches occurring since 1993, rapidly leading to difficulties in littoral communities and their infrastructure. Ocean surface temperatures have risen by at least 0.70°C and oceans have absorbed more than a quarter of CO_2 produced by humans, both leading to acidification and deoxygenation of the ocean, problems that lead to deterioration of marine ecosystems – a significant issue given humanity's absolute dependence on the sea [3,4].

With these two motivating threats, the United States Department of Energy has released goals to drive research towards low-cost, compact, and lightweight hydrogen storage systems and fuel cells [5]. In considering fuel systems from a perspective of energy density, two major elemental systems are noted for expanding boundaries (see Figure 1-1): hydrogen and aluminum, which have exceptionally high gravimetric and volumetric energy densities, respectively.

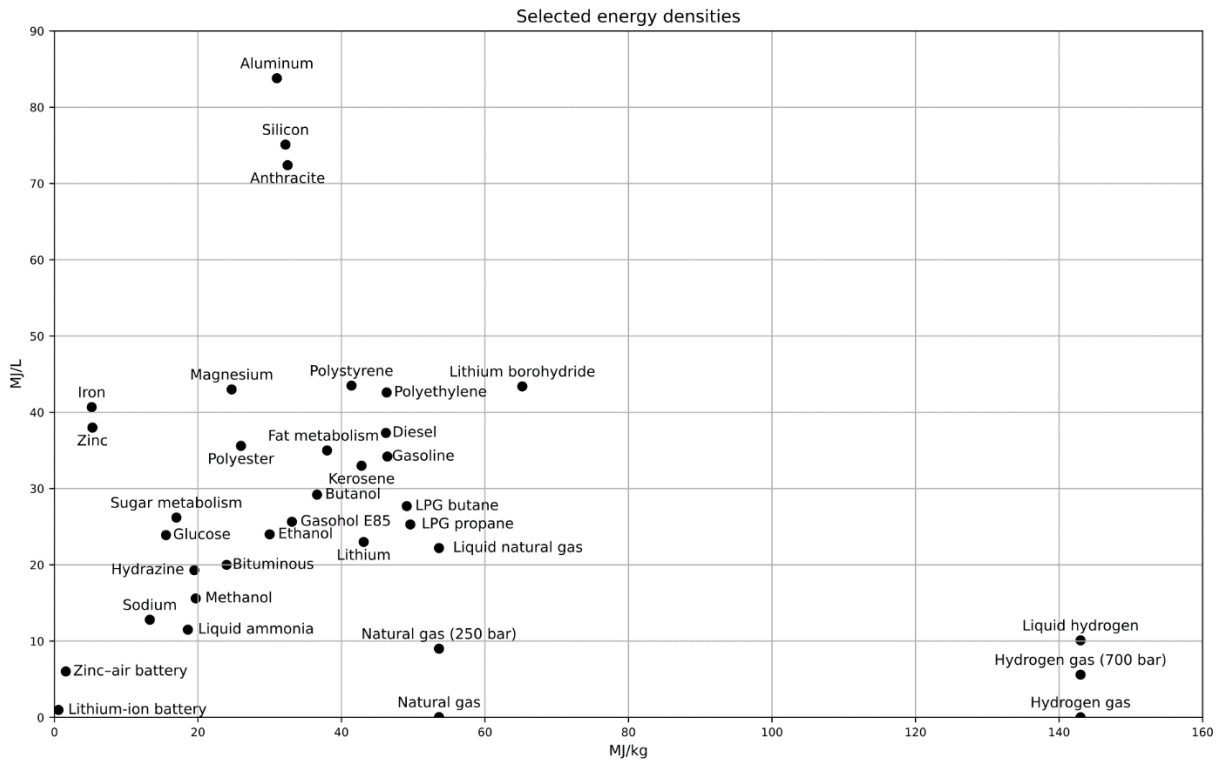

Figure 1-1: Energy densities of selected fuel systems [6]

While hydrogen has a low volumetric energy density, its gravimetric density is far greater than that of more commonly used fuels, and its reaction with oxygen in air produces only water, a more environmentally friendly combustion reaction than that of hydrocarbon-based fossil fuels. Whereas fossil fuels (gasoline, diesel, and natural gas) have gravimetric energy densities of 42-55 MJ/kg, hydrogen holds 120-142 MJ/kg (depending on the phase of the water reaction product) [7]. Its applications include hydrogen fuel cells and internal combustion engines to create electricity or mechanical work. Currently, hydrogen is produced by either steam-methane reforming (stripping a hydrogen from mined methane, CH_4) or electrolysis, both of which have high CO_2 costs [8].

A greater barrier to hydrogen's widespread usage, though, is storage and the affected energy density. Hydrogen may be stored in myriad ways, but the most common are as a compressed gas or supercooled liquid. At standard temperature and pressure, the volumetric energy density of hydrogen gas is only 10.7 kJ/L [9]. Pressurizing the gas at ambient temperature allows for storage at 700 bar, where 5.6 MJ/L is possible [10]. Liquid hydrogen may reach 8 MJ/L, but this is still significantly less than gasoline's 32 MJ/L and requires storage at 20 K [11]. Both

storage systems require additional weight of the storage tank and pressurizing or cooling mechanisms, lowering their hydrogen weight percentage, particularly for gaseous storage. The dangers these storage systems pose are significant, both from the physical status of highly-pressurized gas or extremely low-temperature liquids, and from the ease at which any hydrogen leaks can ignite in air, causing catastrophic explosions [12]. These difficulties make alternative hydrogen storage methods attractive, giving way to considering the use of aluminum.

Aluminum, like many elements, is capable of being oxidized by water to form hydrogen gas and expel heat. It holds a gravimetric energy density of 31 MJ/kg (somewhat less than fossil fuels), but a volumetric energy density of 84 MJ/L – over 2.5 times that of gasoline [13]. The reaction between water and aluminum is thermodynamically favorable and exothermic, forming one of three products by the following reactions:

$$Al + 3\,H_2O \rightarrow \frac{3}{2}H_2 + Al(OH)_3 \tag{1.1}$$

$$Al + 2\,H_2O \rightarrow \frac{3}{2}H_2 + AlO(OH) \tag{1.2}$$

$$Al + H_2O \rightarrow \frac{3}{2}H_2 + Al_2O_3 \tag{1.3}$$

Most metals react with water to form hydrogen gas and metal hydroxides or metal oxides in a process generally known as corrosion. These reactions occur over long periods of time (on the order of millimeters per year) and continuously eat into the bulk of a metal. The most recognizable of these reactions is iron's production of rust. In a few cases, aluminum being one, metals instead form passive oxides. This reaction is extremely quick (on the order of less than a second) and penetrates only a few atoms deep. The oxide layer formed is a hard crust which acts as a barrier to prevent any further oxidation of the bulk material, creating a "practical" nobility for the element. Aluminum is one of these metals of practical nobility. While this trait is extremely useful in structure and machine design, it is the main inhibiting factor for using aluminum as a hydrogen-generating fuel cell [14].

1.2 Development of Aluminum Preparation Methods

Numerous attempts have been made to overcome the passivity of aluminum for its use as a fuel. In 1895, Hans Goldschmidt patented thermite reactions, small explosions of metals and metal oxides, especially of aluminum, which are today used for metal joining, warfighting, and pyrotechnic displays [15]. Over the past twenty years, researchers have focused on reactions between aluminum and water, trying many novel techniques to bypass the passive oxide layer. Similar to thermite, researchers have attempted to use reactions of nanoscale aluminum powders and oxygen [16], or similar particles suspended in a slurry such as JP-10 jet fuel [17]. While these reactions produce high volumes of thermal energy, the stability of nanoscale powders is a challenge, and adding them into a slurry gives rise to the problem of energy dilution.

Seeking solutions for reactions that could take place at standard temperature and pressure, other researchers found that aluminum will react when dropped into highly basic solutions [18,19]. These reactions introduce the issue of containment and disposal or recycling of highly caustic solutions, an issue that is already endemic in the aluminum refinement process [20]. Mechanochemical processes can enable safer reactions with neutral water, where aluminum is milled into a fine powder alongside other metals or salts then reacted with water [21,22]. The widespread use of these powders is still hindered by fear of metal powder storage, and the energy required to produce them is significant.

A new method of alloying aluminum with other metals (zinc, gallium, indium, and tin), published in 2005, resulted in alloys that readily reacted in water at standard temperature and pressure [23]. While this method required significant input energy to melt and cast the alloy, it did spur a new type of aluminum preparation method. Following this discovery, other alloys were designed, some of which were able to be made by dissolving aluminum in liquid metal baths (lithium, magnesium, zinc, tin, and bismuth) [24]. To reduce the energy input and required alloying metals, researchers found that a surface treatment of a liquid metal eutectic (gallium-indium-tin [25] and gallium-indium [13]) was sufficient to "activate" the aluminum for reaction with water.

This reaction of activated aluminum uses a treatment of eutectic gallium-indium (eGaIn) [13,26,27]. eGaIn is 78.6% gallium-21.4% indium by weight with a melting temperature of 15.3°C [28]. The aluminum was activated by adding eGaIn (as little as 4 wt%) to a jar of aluminum pellets heated to 120-200°C for 90-120 minutes. The jar was shaken at regular intervals to fully coat the surfaces of the pellets. After treatment, the samples were stored at room temperature in an inert

environment of argon for a minimum of 3-7 days before reaction. Once added to water, the samples quickly fizzed, producing hydrogen gas and an aluminum hydroxide or oxy-hydroxide slurry by equations (1.1) and (1.2) [27]. This simple activation method has suggested potential uses in electric generation systems and aluminum fuel cell battery systems using the produced hydrogen, and the produced heat may be harnessed for use in water desalination systems.

Greater understanding of the activated-aluminum–water reaction is a necessary step in design and implementation of this technology. While more research is required to fully develop it into a functioning technology, activated aluminum is an energy-dense fuel system that could allow aluminum to be safely transported or gathered without dangers that other aluminum reaction methods pose. Using activated aluminum means that most stages of energy generation are kept on-site, including activation of the fuel, generation of the hydrogen, storage of the hydrogen (if necessary), and usage of the hydrogen through a fuel cell or internal combustion engine. These qualities are of great benefit to the development of safe energy storage, and this thesis aims to do its part in developing this technology.

1.3 Prior Work on the Effects of Strain

When using bulk metal reactants, it is necessary to consider the state of the metal and whether it influences the reaction. Surface effects, including corrosion and anodization, can significantly change how a metal interacts with its environment. Likewise, bulk effects like residual stresses from cold working, or alloying during production or from diffusion, can greatly impact the mechanical and chemical properties of a metal (e.g., highly stressed steels corrode faster than unstressed steels, but stainless steels may not corrode depending on the environment [29]). Some research has explored preliminary relationships between stress and the activated-aluminum–water reaction [13]. In this study, after annealing plate aluminum (1100 alloy), the samples were rolled to various thicknesses (and strain levels), treated in an eGaIn bath, wiped of excess eGaIn, then the hydrogen yield was recorded as a percentage of the expected amount (see Figure 1-2).

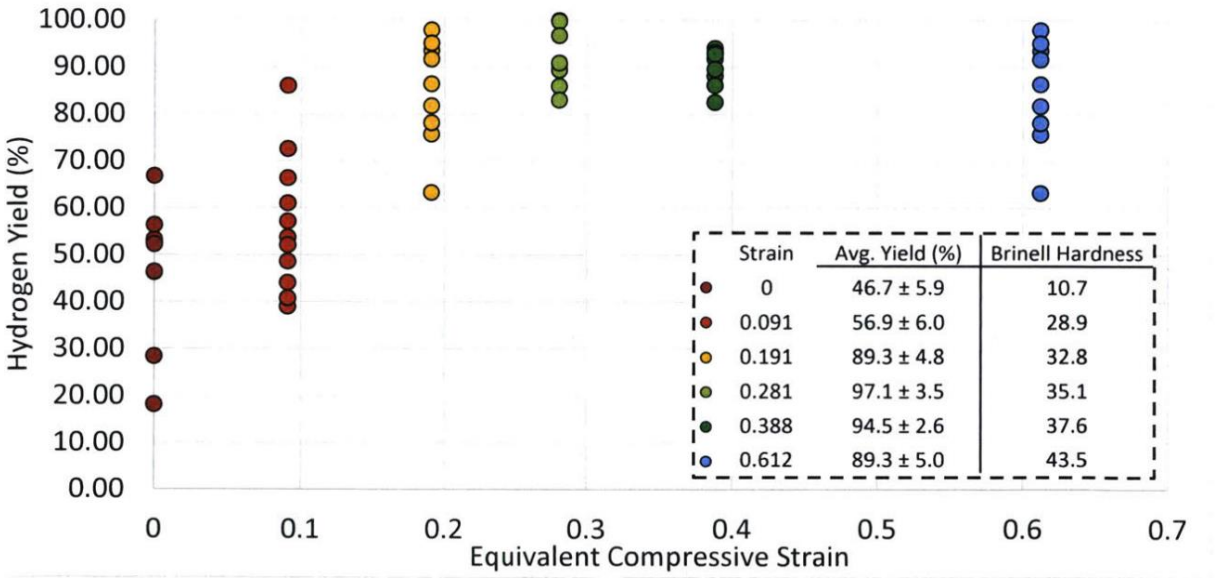

Figure 1-2: Hydrogen Yield v Strain for cold-rolled plate 1100 Aluminum

This work also compared the effects of tensile and compressive stresses by reacting a sample strained under three-point bending, where one side of a sample is under tensile stress and the other is compressed. No discernible difference was noticed between the reaction on either side of the sample [13].

A subsequent study considered the effects of ionic solutions on the reaction at both macro- and micro-scales [27]. By first testing samples using DI water as a reactant, then using additives of salts (NaCl, KCl, $MgCl_2$, $CaCl_2$, and $Al_2(SO_4)_3$) in various concentrations, a number of effects

are seen. One, the eGaIn was then recoverable from the product slurry when it was not under DI water conditions. This is especially important as the cost and reserves of gallium and indium could be prohibitive to the activated aluminum technology. Two, the reaction slowed from a DI water reaction occurring within minutes to a modest ionic solution reaction taking multiple hours to complete (see Figure 1-3). This issue, however, is countered by results from the Lincoln Laboratory at the Massachusetts Institute of Technology that show low concentrations of a caffeine additive may act as a catalyst by accelerating the reaction to under an hour – still slower than a DI water reaction, but a manageable time scale for energy generation. Three, the hydrogen yield dropped by a modest amount, less than 10% of the theoretical hydrogen yield for the aluminum reactant mass. Four, by using water with various solutes, especially 3.5% salinity NaCl and KCl, it is shown that seawater is not only an acceptable reactant alternative to ultrapure water, it provides the benefits of eGaIn recovery and reuse and of adaptability of the reaction to use in various geographic locations and infrastructure levels.

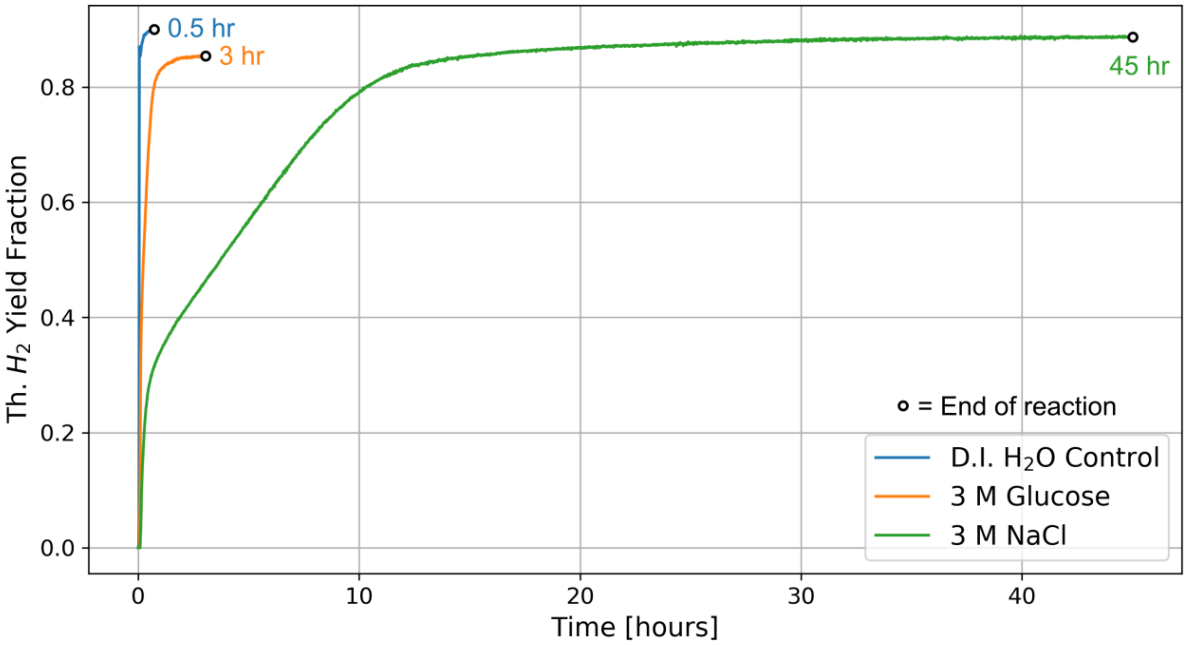

Figure 1-3: Total hydrogen progression as a fraction of theoretical amount from activated aluminum reactions in various solutions [27]

The results of these two studies lead to the questions of how strain affects the reaction for reactor design, and whether using ionic solutions as opposed to DI water will change that effect, as mentioned in the guiding questions posed at the beginning of this chapter.

A final motivating observation also came from the same study [27], when, in imaging the first stages of the reaction in a Scanning Electron Microscope (SEM), an "exfoliation," or delamination, of the aluminum sample was found. By exposing activated aluminum samples to humid environments, the first stages of the reaction were able to be seen using SEM. The images, reproduced in Figure 1-4, are reminiscent of residual stress patterns in metals. This merits exploration into how the reaction proceeds on a microstructural level at different strain levels and leads to the final question guiding the experiments of this thesis.

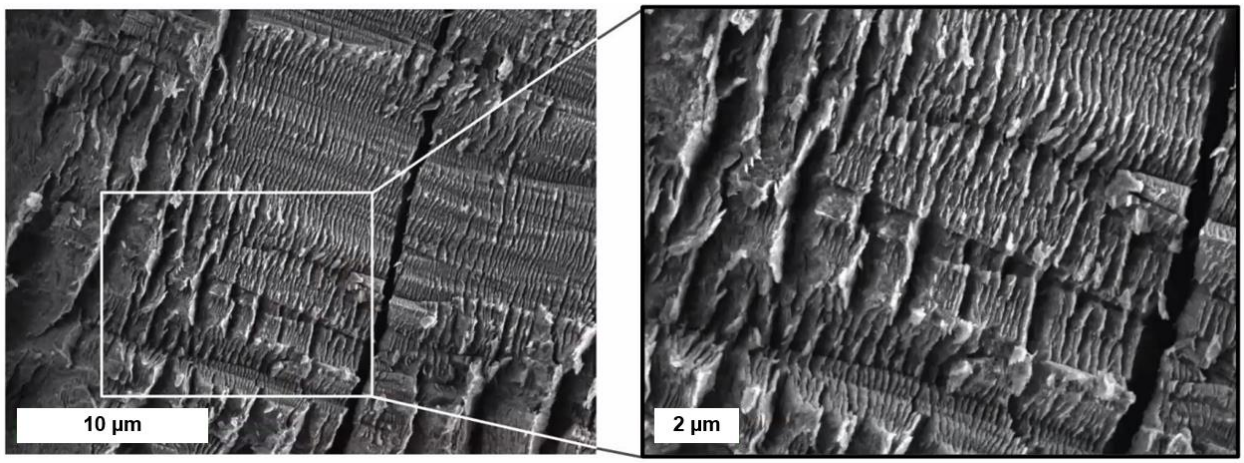

Figure 1-4: The initial stage of activated aluminum disintegration in water reactions, where a delamination process occurs [27]

The questions posed at the beginning of this chapter, exploring the effects of stress on reactions in both DI water and simulated seawater, and at both macroscopic and microscopic scales, are addressed in Chapter 2: Development of Methodology and Chapter 3: Results and Discussion of Strain Effects, and their answers are summarized in Chapter 4: Conclusions and Future Work.

Chapter 2: Development of Methodology

In order to quantify the effect of stress on the reaction of activated aluminum in water, it was necessary to develop a testing methodology that would allow for precise control of residual stresses yet would measure the reaction in a comparable way to previously published experiments. Literature has detailed procedures for conducting hydrogen yield tests [13,26,27]. These tests have primarily mixed small, treated aluminum spheres with water in a flask connected to an isobaric, inverted graduated cylinder immersed in water for hydrogen production measurement. One variation [13] used annealed plate stock rolled to various thicknesses to create residual stress.

Iterating from the previously mentioned experiment, a cold-rolled plate hydrogen yield test was chosen as the primary testing method for this work. It allows hydrogen yield volumes to be compared to a theoretical yield volume to calculate a yield fraction. This can then be compared with previously published results to build a larger body of experimental results on activated aluminum. Additionally, the reciprocal of the reaction rate may be measured and reported as the duration, which can advance the characterization of the reaction and the effect of residual stress.

Controlling the strain levels in the samples was an integral part of preparing tests. Aluminum plate stock was first cut by bandsaw, then the settings for an annealing treatment were determined by testing sample hardness over a variety of heating durations. The sample thickness was first measured, then a rolling mill was used to apply stress in one dimension through the samples. Resulting strains were then calculated by measuring the post-rolled thickness with calipers and comparing it to the original value. Samples needed to be activated without affecting the residual stresses that had been developed, so hardness values were again checked once samples were heated at the temperature and duration of the activation treatment.

Once this method of sample preparation was determined, hydrogen production and microstructural changes were measured following published protocols. Hydrogen yield tests capture the gaseous products of the reaction in an inverted graduated cylinder and compares the experimental and theoretical moles of hydrogen produced. By partially reacting samples in humid air, SEM imaging allows for the first stages of reaction to be observed so that samples with different strain levels may be contrasted at equal levels of reaction progression. Together, these values help to answer the questions of how stress and reactant water types influence the activated-aluminum–water reaction, and how stress affects the reaction at microstructural levels.

2.1 Cold Working Aluminum for Controlled Strain Levels

1100 Aluminum was chosen as a nearly pure alloy, readily obtained from McMaster-Carr. The sample plate obtained has an H14 temper and is quoted to thickness tolerance ±0.007" (0.178 mm) [30]. 1100 Aluminum is codified by ASM International as 99.00% minimum aluminum, 1.0% maximum silicon and iron, 0.05-0.20% copper, 0.05% maximum manganese, 0.10% maximum zinc, 0.05% maximum other elements individually, and 0.15% maximum other elements total. The alloy has good formability and higher strengths than higher-purity alloys [31]. The combination of purity, formability, and accessibility led to this alloy's selection for this work.

In determining an adequate cutting method, the limiting factor was to obtain samples that were approximately 0.3g in mass. This would enable a small, contained reaction that would not exceed the test setup's capacity for H_2 gas evolution. Starting from 1/8-inch (3.175 mm) thick plate stock, a density calculation showed that a 5x7-mm sample would be approximately 0.3g. These samples were cut using a bandsaw (Figure 2-1), and any chips attached to the main aluminum block were removed. While this method did result in variation of the sample masses (an average of 0.279 ± 0.027g), values were still under the 0.3g mass limit and deemed acceptable.

Figure 2-1: Samples pile up on the far side of a bandsaw's blade after being cut from the thin bar of aluminum just in front of the wood push block.

Once physical shaping was complete (i.e., actions that would cause residual stresses apart from the controlled rolling), it was necessary to anneal the samples to remove all history of stress from the microstructure. First, the samples were cleaned by immersing them in a sonicating bath of isopropanol followed by manual mixing to ensure the removal of any dirt and grease from production, transportation, or cutting.

Several test samples were first used to determine a proper annealing method for the experiment. Using the ASM instruction heat treatment temperature of 345°C (653°F) [32], the test samples were placed in a temperature-controlled furnace (Thermo Scientific™ Lindberg/Blue M™ Moldatherm™ Box Furnace) for varied lengths of time. Next, the samples' hardness values were checked with a Vickers Indenter (Leco® MicroHardness Tester LM248AT/Cornerstone® AMH55 L Version 2.8.9) to determine the required duration for annealing. Hardness measurements were read at 500 gf with a 15-second dwell time, and results given are each the averages of six indents over two samples. Samples had no further surface preparation other than cleaning. These results are summarized in Table 2.1. 30 minutes was thus chosen as a sufficient length of time to anneal all the samples with confidence.

Table 2.1: Vickers Hardness values of 1100 Aluminum after various heat treatment times at 345°C

Heating Time [min]	None, Tested As Received	5	10	15	20	30	45	60	90	120
Average Hardness [HV]	40.8	32.6	28.8	24.7	22.8	22.8	23.4	23.0	23.5	21.7

Following the "resetting" of the samples, the final step of preparation was cold rolling. Using a rolling mill (IRM Rolling Mill, model #3050H, 5 hp. Rolls are H13 Tool Steel, 2 Ra finish, 56-58 Rockwell C hardness with diameters of 76.2mm/3.0in), the samples (less some unstrained controls) were compressed in thickness. This compression plastically deformed them and provided a controllable level of strain, a corollary of residual stress and the primary independent variable to be tested. Rolling was executed in incremental steps of approximately 10% of the initial thickness

(0.0125 inches or 0.3175 mm). Samples went through the mill in batches to maintain uniformity across the samples. All samples entered the rolling mill along their major axis. Batches were held together using two pieces of printer paper (Figure 2-2), and thicknesses were checked by calipers (±0.001 in/0.0254 mm) after rolling to verify the target thickness. Thicknesses that measured within a few thousandths of an inch of their target value were considered sufficient. Similar to the annealing step, a small "test" batch was used to verify the rolled thickness to make sure all samples to be used in testing would not be sent through the rolling mill more than necessary. After every 10% decrease in thickness, a group of samples were separated for treatment. Using equation (2.1) for engineering strain, where ε represents strain and t represents thickness,

$$\varepsilon_{eng} = \frac{t_{initial} - t_{final}}{t_{initial}}, \tag{2.1}$$

the groups of samples were categorized by approximate engineering strain value. Two items are noted here. One, the groups of similar strain levels produced still had significant variation in their thicknesses despite the entirety of a group going through the rolling mill in one paper-bound batch. Before treatment, each sample's thickness was measured to determine its precise residual stress level, so some variation for each general strain level can be seen in the resultant plots. Two, strain is a unitless ratio, but is often given units of "strain." Thus, each decrease of 10% of the initial thickness on the rolling mill equates to -0.1 strain, where the negative sign indicates a decrease in the dimension, or a compressive strain. However, for simplicity's sake and for easier comprehension of plotted results, all strain levels for the remainder of this thesis will be the absolute value.

After rolling, samples were cleaned once again in a sonicating bath of isopropanol before moving on to hydrogen yield experiments. Examples of samples produced are provided in Figure 2-3.

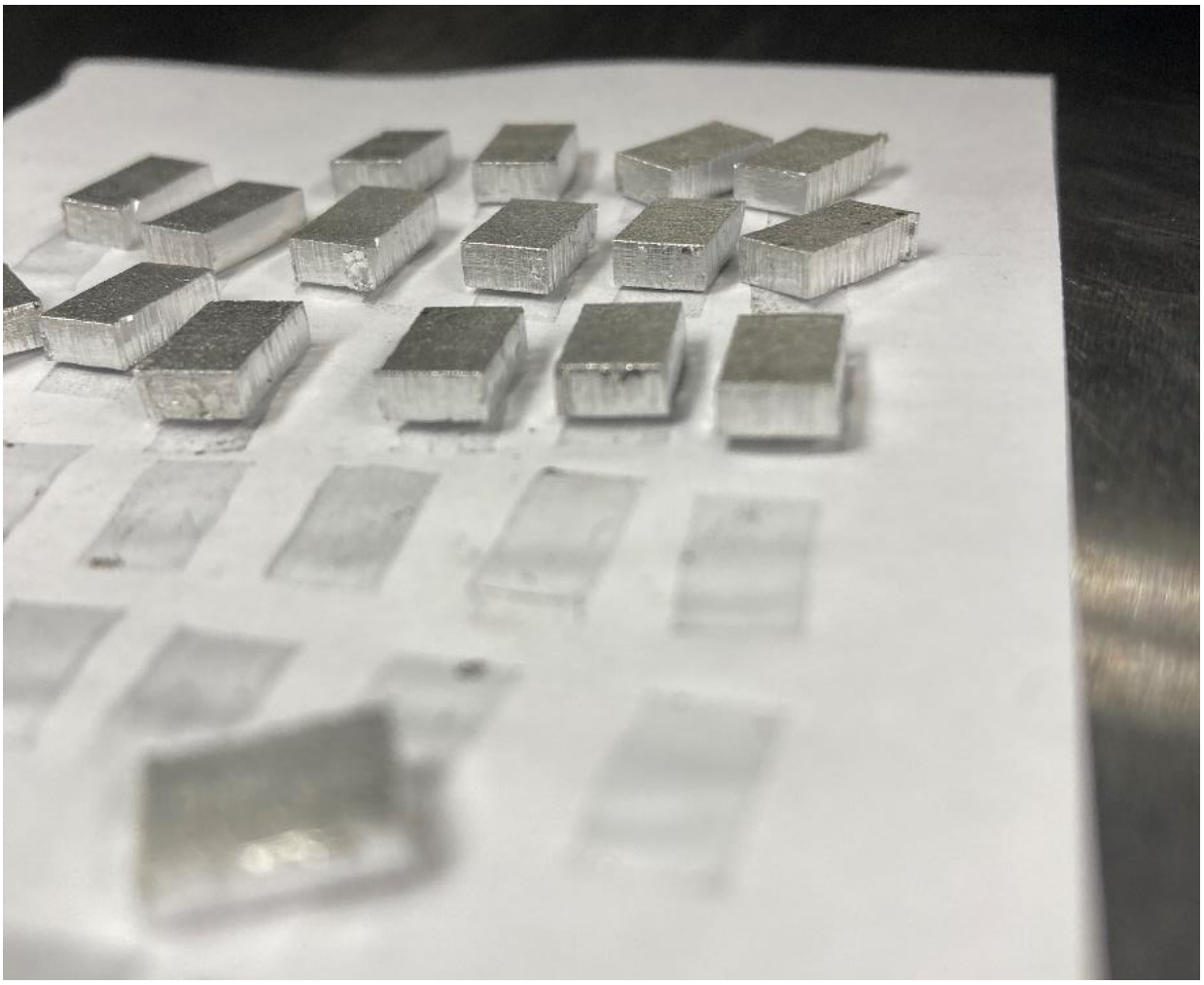

Figure 2-2: Samples sitting on a paper used to contain them as they went through the rolling mill. In the foreground, compressed regions of the paper show where another group of samples had laid before reaching their desired thickness.

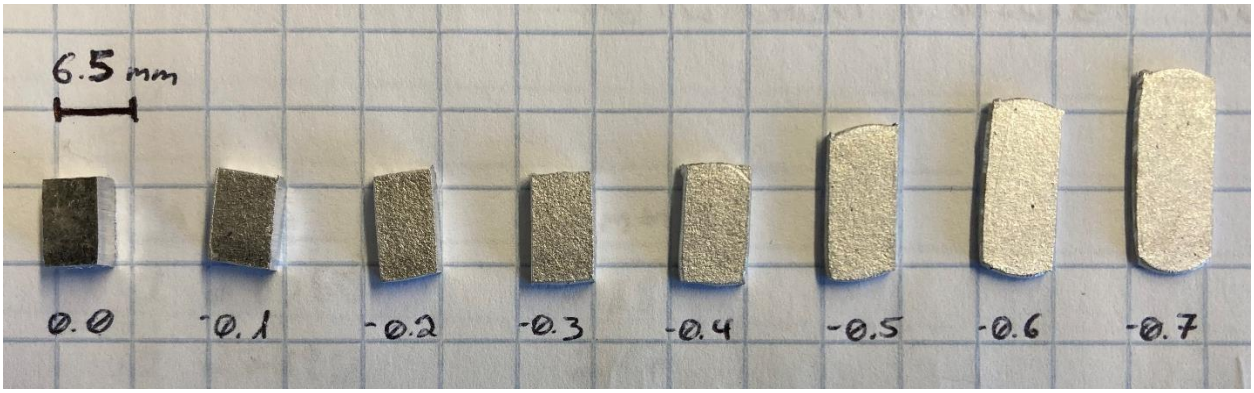

Figure 2-3: Annealed, rolled aluminum samples listed by approximate strain level

2.2 eGaIn Aluminum Activation Process

As discussed in Chapter 1, Background, multiple studies have been performed by previous researchers to activate aluminum with eutectic Gallium-Indium (eGaIn) at near-room-temperatures. A method has been developed to treat aluminum pellets by immersing them in a heated bath of eGaIn for a period of time – on the order of a couple hours – during which the containing jar is periodically shaken to fully wet the surface of the pellets with the eGaIn [13,26,27].

While this general method of an eGaIn surface treatment was chosen as the original idea to expand upon, a few modifications were introduced for the purposes of testing the effect of strain. One, the treatment temperature and time was minimized to prevent annealing the stressed samples. Two, the variation in mass between samples caused by the cutting method dictates that each individual sample be tracked through treatment so that its mass pre- and post-treatment may be compared and its eGaIn wt% can be calculated.

To achieve these modifications, a few informal trials were conducted that varied temperature and eGaIn addition amount and method. Samples were treated at room temperature, 120°C, and 200°C. eGaIn was added to the samples in various was, including by placing the samples in liquid metal pools, allowing beads of liquid metal to contact the sample edges, pipetting various amounts of eGaIn onto the surface of the sample, and flipping the samples during treatment for more surface coverage. These trials resulted in a treatment temperature of 120°C and an eGaIn addition of 5 µL by pipette to the surface of each sample followed by flipping samples during treatment.

In order to confirm the treatment temperature and time did not significantly anneal the stressed samples, their hardness values were measured. Sample surfaces were prepared by removing the uneven surface (formed by cold rolling) with P4000 grit sandpaper (Buehler Microcut®, 5 µm average grain size). A Vickers Hardness indenter applied 500 gf for 15s, and samples were tested ten times each – five times on either side – and the measurements averaged. Before heating, a 0.7 strain sample had a hardness of 52.9 HV. After 2 hours of heating at 120°C, it measured 52.3 HV. A 0.7 strain sample treated at 200°C for 2 hours had a hardness of 48.9 HV. Compared to an annealed hardness of about 23 HV (see Table 2.1), this heated treatment method has an appreciably small effect on residual stress level. It is noted that these quick trials did not

aim to fully minimize the treatment conditions, only to demonstrate that previously-used methods did not significantly impact the residual stresses produced in the aluminum samples.

In order to keep track of the individual samples, treatment would have to occur in separated regions of the hot plate, and instead of shaking the entire mass of samples as detailed in literature, each sample would be carefully flipped every 15 minutes while remaining in place. This resulted in each sample being placed on its own puddle of eGaIn to coat the largest sides through flipping multiple times. Upon visual inspection after 72 hours of sitting in an argon-filled container, the eGaIn had fully permeated the bulk and the untreated sides of the sample.

The Standard Operating Procedure (SOP) used for treatment of aluminum samples with eGaIn is provided:

1. Weigh individual aluminum samples.
2. Place on a hot plate set to 120°C, elevated by a thin glass dish or plate.
3. After 30 minutes, pipette 5 µL eGaIn onto the surface of each sample. Not all of the eGaIn will stick to the sample, that is accepted.
4. Every 15 minutes, flip the sample, making sure to keep the sample in the same location. Before and after flipping, a small amount of force pressing the aluminum to the glass is helpful to encourage the eGaIn to wet the lower surface of the aluminum.
5. Conclude the heat treatment at a total of 120 minutes of heating (for a total of 5 flips).
6. Immediately place the samples in a sealed container and fill with Argon gas. Make sure to keep each sample separate in a marked location.
7. Allow at least 72 hours for grain boundary permeation of the eGaIn.
8. Before testing, make sure to weigh the sample to determine the treated mass and eGaIn addition percent.

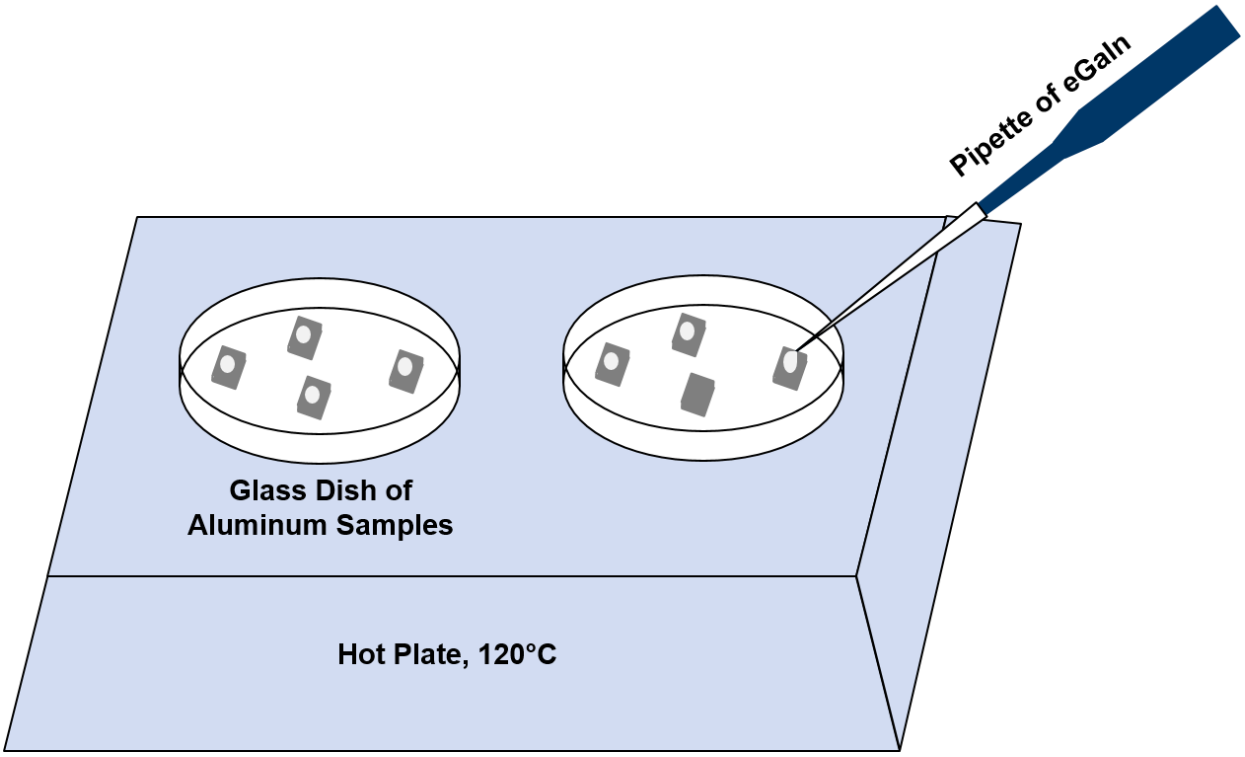

Figure 2-4: Diagram of eGaIn addition during sample heating (SOP Step 3)

For this procedure, no eGaIn was removed from the surface of the sample after treatment. This resulted in some balled liquid metal on the surface of the samples even after the 72 hour rest period. Some aluminum diffuses into this eGaIn coating, visually observed by the discoloration from a reflective, metallic sheen of pure eGaIn to a hazy, matte surface once impregnated with aluminum. In order to not lose any of the original aluminum mass, the excess eGaIn coating was reacted along with the aluminum sample.

In addition, while 5 µL of eGaIn is pipetted onto the top of each sample during heating as it is an ideal volume to allow easy treatment of each sample individually, the actual uptake volume is significantly less than 5µL. A significant amount of eGaIn sticks to the inside of the pipette tip, and more remains on the surface of the glass dish after the treatment. As shown below in Figure 2-5, though, the amount of eGaIn absorbed by the aluminum samples has a uniform distribution across strain levels and samples. The one exception to this trend are the 0.7 strain samples which all absorbed more eGaIn than the trend at other strain levels. This exception is not expected to have a measurable effect on the results, as the trends seen in Figure 3-1 and Figure 3-3 of the next

chapter do not appear to have any large step inputs at the 0.7 strain level. This is noted as the different strain samples absorb approximately the same amount of eGaIn, irrespective of their having significantly different surface areas that are being treated with eGaIn – higher strain samples' major faces (the two originally treated) have multiple times the area compared to major faces of samples with no strain.

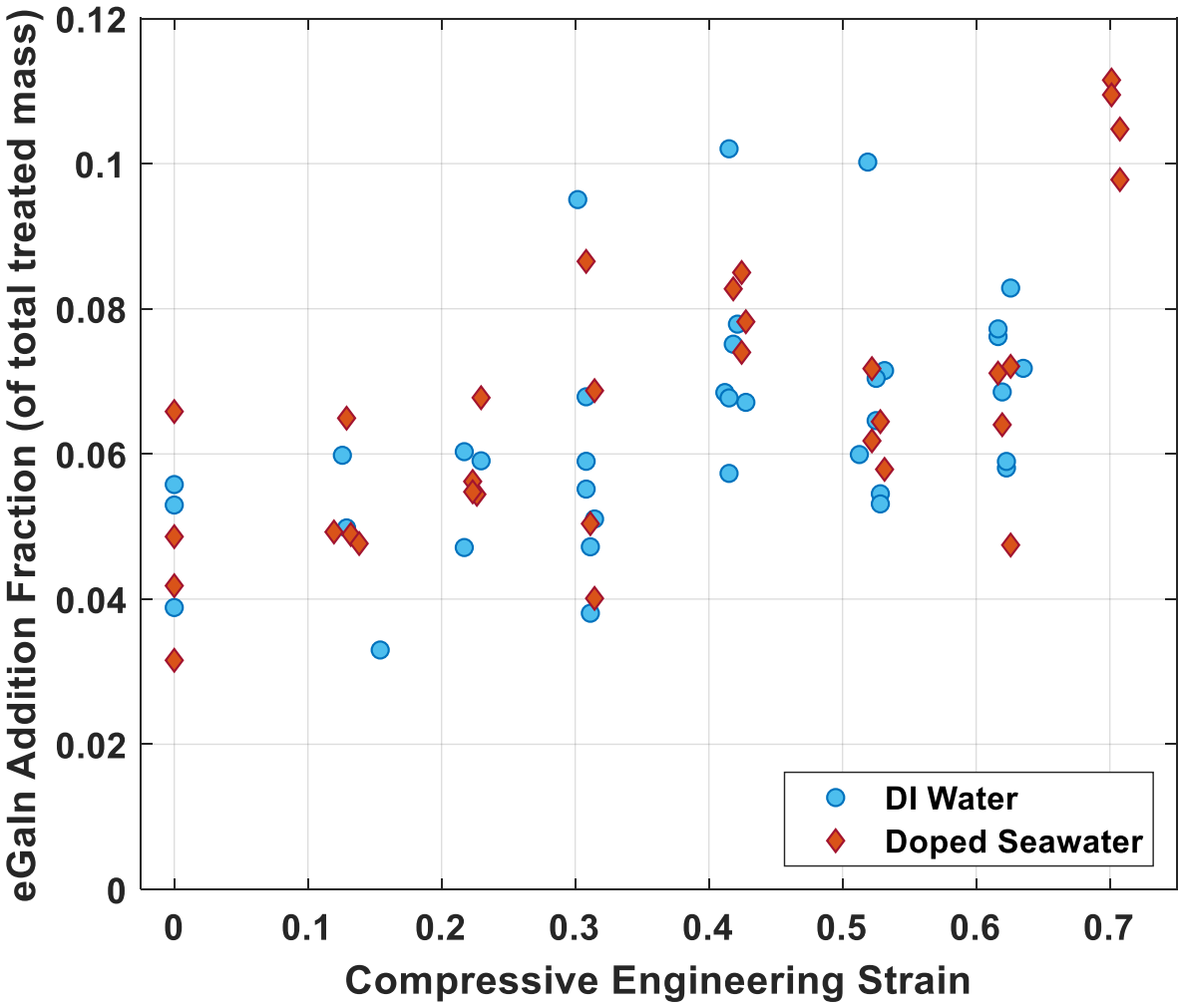

Figure 2-5: eGaIn addition as a weight percent of the treated sample mass, plotted by strain level. Note the only outlier to a uniform distribution across strain levels is at 0.7 strain. Doped seawater refers to the reactant water used as detailed in Section 2.4,

Types of Reactant Water.

2.3 Hydrogen Yield Testing

To determine the reaction yield fraction and reaction duration for activated aluminum in water, the gaseous product is captured in an inverted graduated cylinder filled with water, assembled in accordance with literature [13,26,27]. The reaction occurs in a Buchner flask. The flask's stopper has a feed connected to a syringe that feeds water into the flask. The flask's outlet flows through a tube with marked volume intervals along its length. The tube's end is fixed directly underneath the mouth of the inverted graduated cylinder in its water bath, which is open to the atmosphere. In this way, a sample of activated aluminum can be dropped into the Buchner flask, and the syringe plunger can be depressed so that a controlled volume of water is added to the activated aluminum sample. The reaction's gaseous product flows through the tube and up into the inverted graduated cylinder, measuring the gaseous product's volume (See Figure 2-6 and Figure 2-7). A stoichiometric ratio of eight to ten times the required water to added water has been reported as necessary to cool the reaction and maintain the chemical mechanisms [27]. In order to maintain a stoichiometric ratio of at least 8, 5 mL of water are used for the reaction, as per equation (2.2), where *V* represents volume, *n* represents moles, *M* represents molar mass, *m* represents mass, and 3 is the stoichiometric reaction ratio from equation (1.1), which is greater and therefore the extreme case over equation (1.2).

$$3 \cdot \left(V_{water}[mL] \cdot \rho_{water} \left[\frac{g}{m^3}\right] \cdot M_{water} \left[\frac{g}{mol}\right] \cdot \frac{1e6\ m^3}{mL} = n_{water} \right) : n_{Al} = \frac{m_{Al}}{M_{Al}} \qquad (2.2)$$

In order to ensure the completeness of the reaction, which can be stalled in an aggressively mixed slurry of solid reaction products, and to aid in the reaction's cooling towards equilibrium for measurement, and an additional 5 mL of water are added to the beaker once the reaction appears to have been completed. A reaction is marked completed once the product slurry is no longer producing visible bubbles upon agitation. Following the reaction, the slurry of products is observed for eGaIn precipitation then filtered through a sieve (ASTM E-11 Specification, No. 70, Opening size of 212 µm/8.3 thou) for closer visual inspection.

The volume in the graduated cylinder must be modified for two environmental factors. One, the atmospheric temperature and pressure force the evaporation of some water into the

cylinder that must be subtracted from the measurement. Two, in reactions that take place over the course of about 20 minutes or less, the reaction releases heat too quickly to reach equilibrium by the time measurements are marked down at the end of the test. In order to remedy this, the Buchner flask, containing the slurry of solid products of the reaction suspended in the excess water, including the additional 5mL of water added, may be placed in a basin of cool water gently circulating, making sure not to wet the flask in a way that would introduce any additional water to the reaction. This quickly cools the product slurry towards equilibrium, creating a vacuum in the free space of the flask and the outlet tube. The vacuum pulls water from the cylinder's basin up into the outlet tube, where markings of the tube's volume can be read to show how much becomes filled by the water.

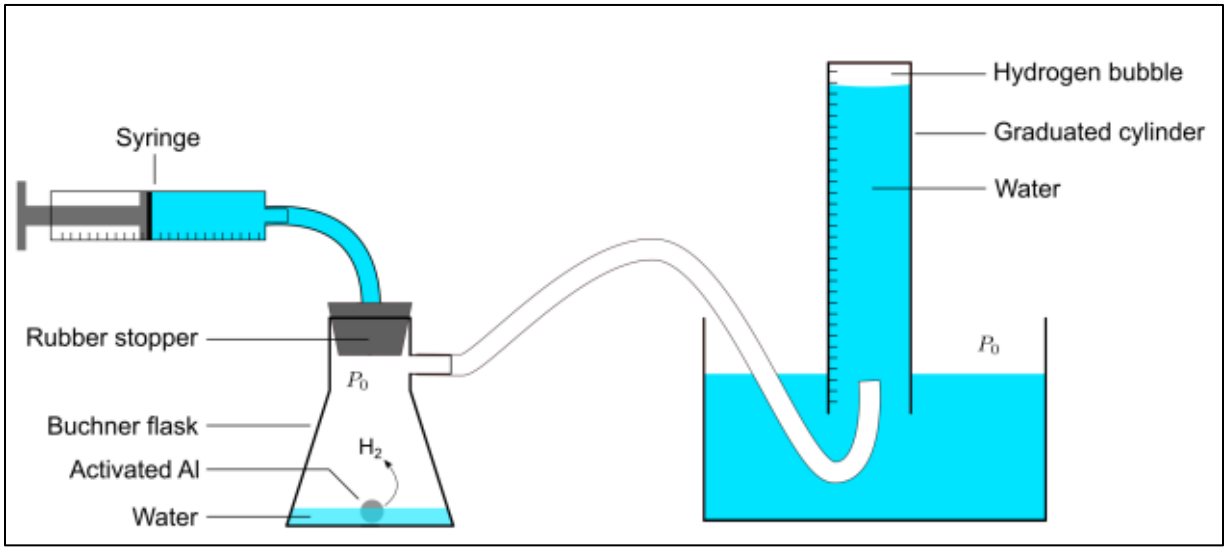

Figure 2-6: A diagram of the inverted-graduated-cylinder, hydrogen-capture test setup [27]

Figure 2-7: Image of the test setup used. In the back right are beakers of DI water for refilling the syringe and wetting the rubber stopper and a rectangular dish of tap water to cool the Buchner flask after the reaction.

The yield fraction of hydrogen gas produced is defined as the moles of experimental hydrogen produced divided by the theoretical moles able to be produced by the mass of the aluminum sample. The theoretical moles ($n_{theoretical}$) produced are calculated as

$$n_{theoretical} = \frac{3}{2} \cdot \frac{m_{Al}}{M_{Al}}, \tag{2.3}$$

where m_{Al} is the measured mass of the specific aluminum sample prior to treatment with eGaIn, M_{Al} is the molar mass of aluminum, and the coefficient of 3/2 is the stoichiometric ratio from Equations (1.1) and (1.2).

The experimental moles of hydrogen produced can be calculated using the ideal gas law,

$$n_{experimental} = \frac{p_{H_2} V_{modified}}{R\, T_0}, \tag{2.4}$$

where R is the ideal gas constant and T_0 is the ambient temperature of the room. The ambient temperature is considered sufficient as the hydrogen gas is bubbled through the graduated cylinder's water basin and the Buchner flask is cooled in another water basin, both of which are at ambient temperature. p_{H_2}, the partial pressure of hydrogen, and $V_{modified}$, the calculated volume of H_2 gas, are described below.

The partial pressure of hydrogen gas is modified from the ambient pressure to which the graduated cylinder's water basin is exposed using Equation (X), below.

$$p_{H_2} = p_0 - p_{H_2O}, \tag{2.4}$$

where p_0 is the ambient pressure of the room and p_{H_2O} is the saturation pressure of water vapor calculated at the ambient temperature using the Antoine Equation [33].

$V_{modified}$ is the read volume of gas in the graduated cylinder less the volume of the tube filled with water (due to the thermal contraction effect described previously in this section) and the 10 mL of water added to the flask. The volume of the Buchner flask is not added to this as it is originally filled with air, and that same volume of air remains intermixed with the gaseous product after the reaction.

2.4 Types of Reactant Water

Two batteries of experiments were conducted using the described hydrogen yield test, each with a different type of water. The first battery used DeIonized (DI) water to minimize the amount of incidental chemicals in the reaction. The second battery used DI water doped with 0.6M NaCl (Sigma-Aldrich®, >99% purity) and 0.1M caffeine (Sigma-Aldrich®, >99% purity). 0.6M NaCl solutions (35g/L NaCl, or 3.5% salinity) can be used as a laboratory approximation for seawater, which is 3.5% salinity. Though seawater is not entirely NaCl, published experiments using equal-molarity solutions of various salts (NaCl, KCl, $MgCl_2$, $CaCl_2$) showed that the hydrogen yield, reaction duration, and eGaIn recovery were approximately the same regardless of species of salt added [27]. By emulating seawater in this thesis, the design of energy-generation systems that use activated aluminum fuel is aided, as many potential reactors would most easily be placed next to seawater, such as a disaster-relief site that could use aluminum scrap and seawater to generate electricity for the community. However, the addition of ions to the reaction's water significantly slows the reaction. Experiments at MIT's Lincoln Laboratory have unpublished preliminary results that suggest an additive of caffeine may act as a catalyst to speed up the reaction, even at low concentrations. After a few tests to measure the necessary amount of caffeine to contain the reaction duration to less than one hour, 0.1M caffeine was deemed sufficient. Note both types are referred to as the reactant "water" in this thesis.

With the eGaIn treatment SOP and the water dopants determined, the activated aluminum was ready to be tested. With eight levels of strain produced and two types of water, the following matrix was tested: In DI water, strain levels 0.0 – 0.6 were tested in triplicate. In caffeine-doped seawater, strain levels of 0.0 – 0.7 were tested in quadruplicate. Noting the tests in DI water at higher strain levels produced results with greater variation than lower strain levels, four additional tests were conducted for DI water strain levels 0.3 – 0.6, for a total of seven times.

While 5mL was the prescribed amount of water to be added to the reaction, in two conditions, it was observed the additional 5mL of water, set aside to verify the completion of the reaction and begin the cooling process, was in fact required to complete a significant part of the reaction. One, the reactions in DI water with high strain levels (all 0.7 and occasionally 0.6) were observed to be so violent that the partially reacted aluminum sample would be flung to the top of the flask by the power of the reaction occurring beneath it. There, it would sit, supported by the slurry of AlOOH produced, dried to a hard layer by the heat of the reaction (see Figure 2-8, below).

The additional 5mL of water was then required to complete the reaction, and the duration measurement includes the reactivity shown after the additional water was added.

Figure 2-8: A sample of aluminum with a high strain level of 0.6, reacting in DI water, has been thrown to the top of the products and dried out, prematurely halting the reaction.

Two, all seawater reactions formed a hard crust that was dried out by the heat of the reaction. In all of these reactions, the additional water was added during the reaction to hydrate and break the crust, resulting in some further reactivity. At low strain levels (~0.0 – 0.4), this is

just seen as a hard crust. At higher strain levels (~0.5 – 0.7), the reaction appeared to have grown out along tendrils in appearance like bleached coral. Examples of these crusts can be seen below in Figure 2-9.

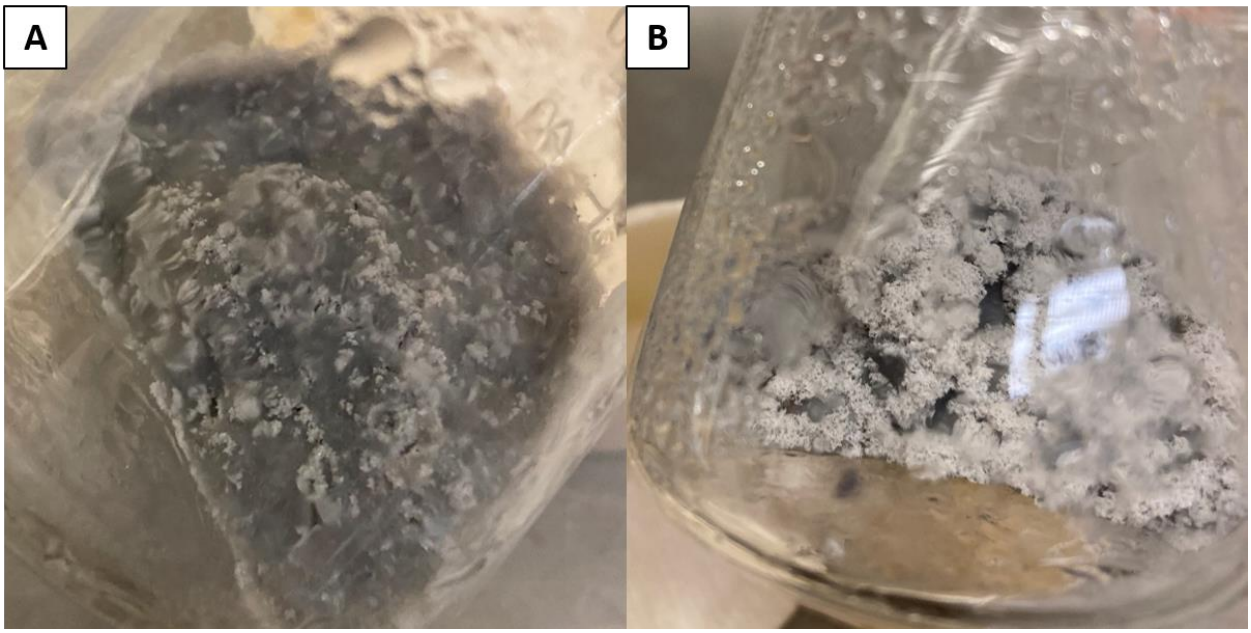

Figure 2-9: A) A crust of products has formed in a reaction of seawater and 0.1 strain aluminum. B) A characteristic crust at a higher strain level of 0.6. In both cases, only 5mL of water had yet been added to the flask.

2.5 SEM Imaging

In addition to the hydrogen yield tests, SEM images were taken to observe microstructural trends and clarify findings. Samples were imaged using a Zeiss Merlin Field Emission SEM in secondary electron mode operating at 3 kV and 100 pA. One sample was scanned with Energy-Dispersive X-ray Spectroscopy (EDS), which was done in conjunction with the SEM imaging at 20 kV and 2nA. All measurements were taken within a working distance range of 6-8 mm. The X-ray intensity measurements were corrected using the ZAF method, implemented with Apex EDAX software, which corrects for errors resulting from atomic-number-dependent stopping power (Z), absorption of lighter element's X-rays by heavier atoms (A), and induced secondary fluorescence (F). The corrected measurements allow for the SEM image to be evaluated pixel-by-pixel to determine elemental composition.

Samples imaged with the SEM were a 0.0 strain sample and a 0.6 strain sample, intended to demonstrate the effect of strain on microstructural reaction progression. These samples were treated with eGaIn and aged as previously described in Section 2.2, the eGaIn Aluminum Activation Process, then reacted by sealing in a container which contained an open vial of DI water. This resulted in a humid environment which began the sample's reactions at a controlled pace. The 0.0 strain sample was reacted for three hours, and the 0.6 strain sample was reacted for one hour. Samples were then attached to an aluminum sample holder with graphite tape and placed in the SEM. Additional control samples of 0.0 strain and 0.6 strain were neither treated with eGaIn nor polished, but imaged in the SEM in the same way to provide a baseline for the reacted samples.

In order to inspect some filaments seen after high-strain DI reactions, a small amount of reaction product was also imaged. This product was obtained by reacting a 0.6 strain sample in DI water and scooping a small amount of the product slurry onto graphite tape placed on an aluminum sample holder. The product was air-dried for 15 minutes to ensure only solid product entered the SEM for imaging. This filament product sample was scanned using EDS for its elemental composition.

Chapter 3: Results and Discussion of Strain Effects

Following the procedures detailed in the previous chapter to test the matrix of experiments in Section 2.4, Types of Reactant Water the plots produced showed no impact of strain to hydrogen yield but a large acceleration of the reaction at increasing strain levels. Numerical data can be found in the Appendix of Hydrogen Production Data. Unreacted aluminum was seen at high strain levels for DI water reactions and inconsistently in caffeinated seawater reactions. SEM images did not show a strong relationship between strain level and microstructural mechanics of aluminum breakup.

3.1 Initial Results

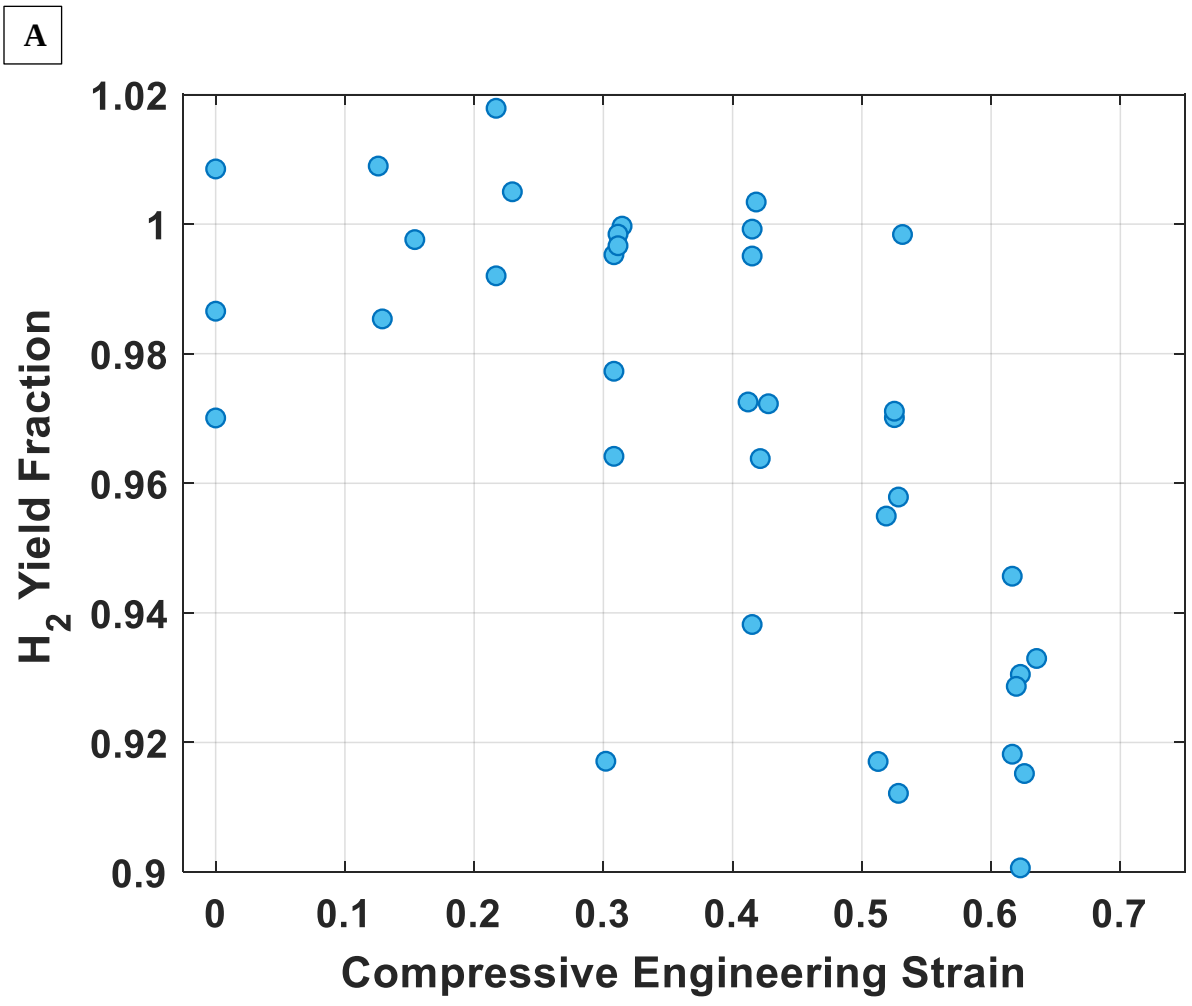

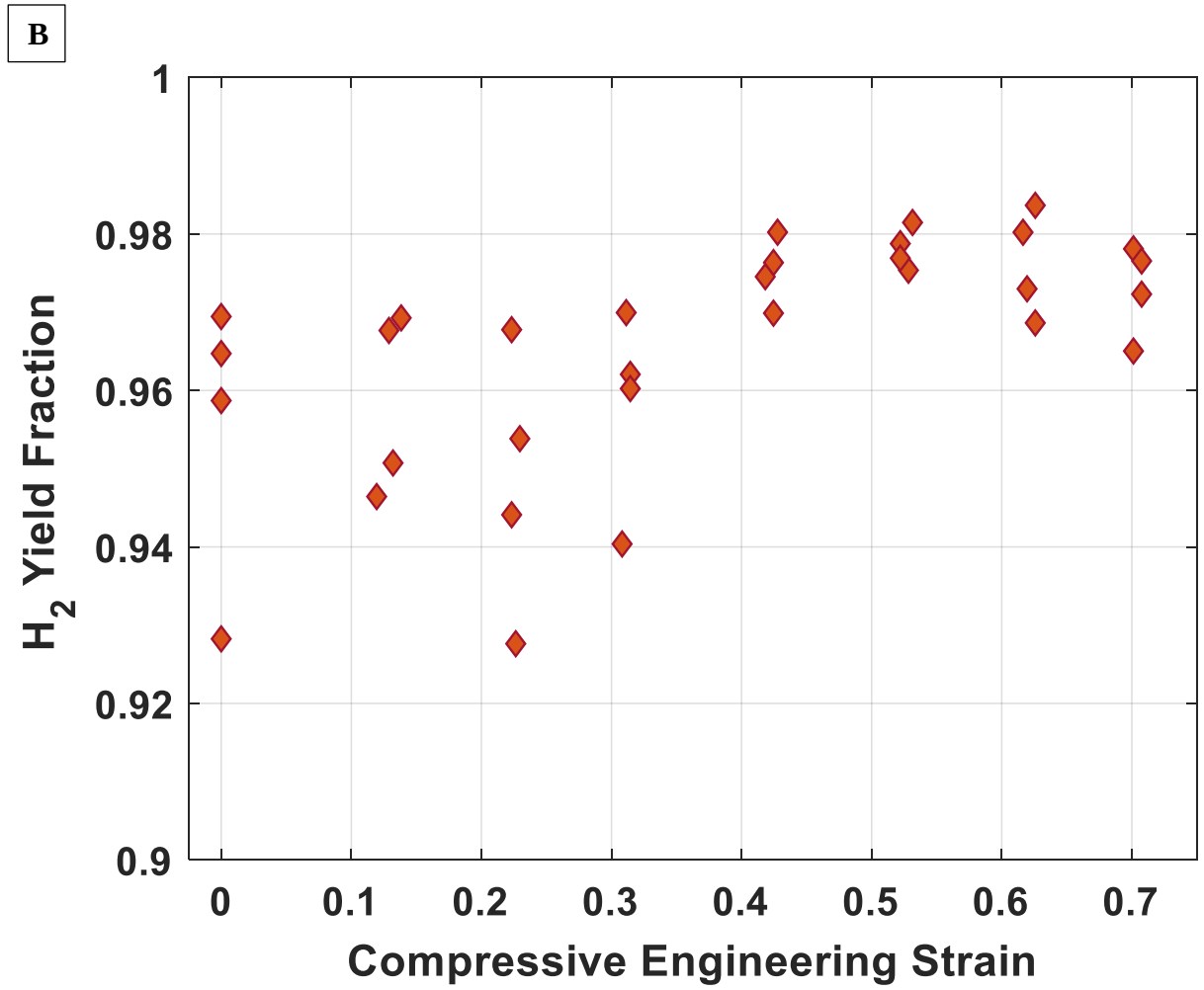

Figure 3-1: Plots of Hydrogen Yield v Strain for A) DI water and B) caffeine-doped seawater

Results of hydrogen yield for both DI water and caffeine-doped seawater do not exhibit a relationship between yield and strain level (Figure 3-1). Measurement error for Yield Fraction was ±0.00917 and ±0.00314 for Strain. In DI water, the reaction is near completion across all strain levels, though with more variation in the higher strain levels. Yield fractions of greater than one occur due to oxidation of gallium. This only occurs in DI water, not ionic solutions such as seawater [27]. Caffeinated seawater reactions stayed constant across the range of strain levels but reached an asymptote around a yield fraction of 0.985 without any visual indication of an incomplete reaction (examples of standard product slurries are seen in Figure 3-2). This trend where reactions in ionized water do not fully produce their theoretical amount of hydrogen gas has also been observed in literature, where a yield fraction of 0.95 ± 0.05 has been obtained with NaCl solution, though at a significantly higher molarity (3.9M) and without caffeine dopant [27].

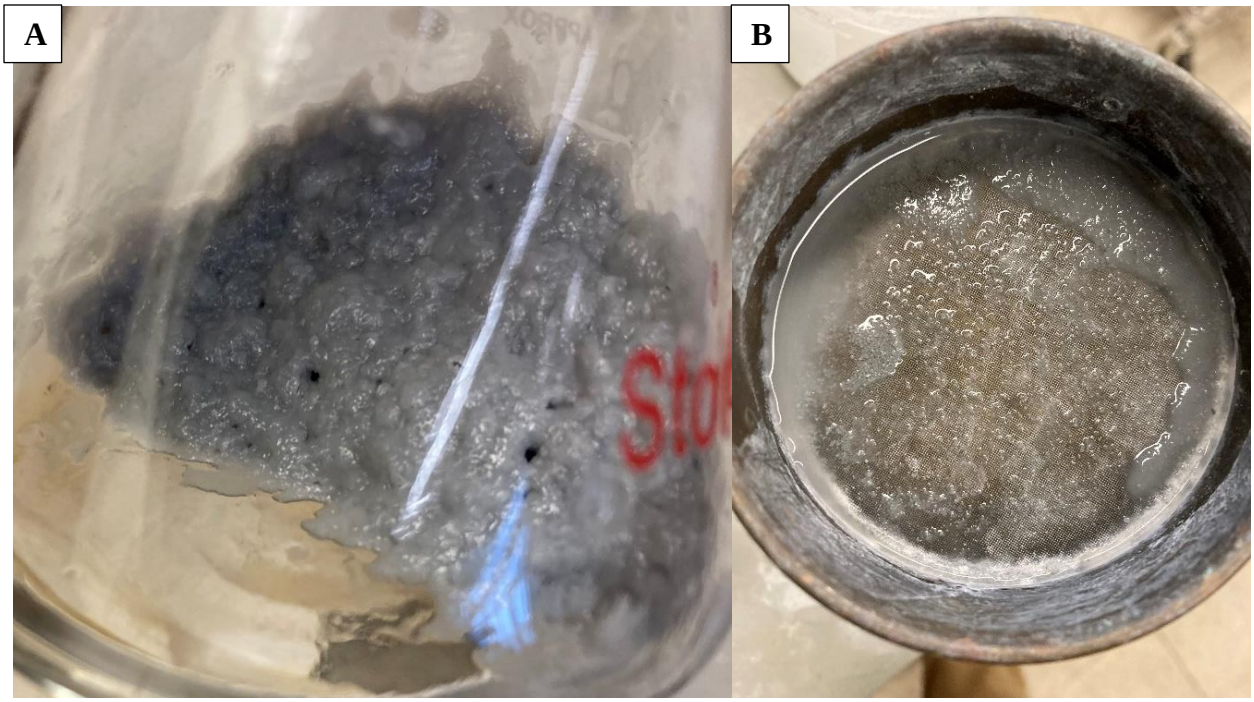

Figure 3-2: Images of a typical post-reaction product slurry, A) in the Buchner flask, B) after filtering through the sieve

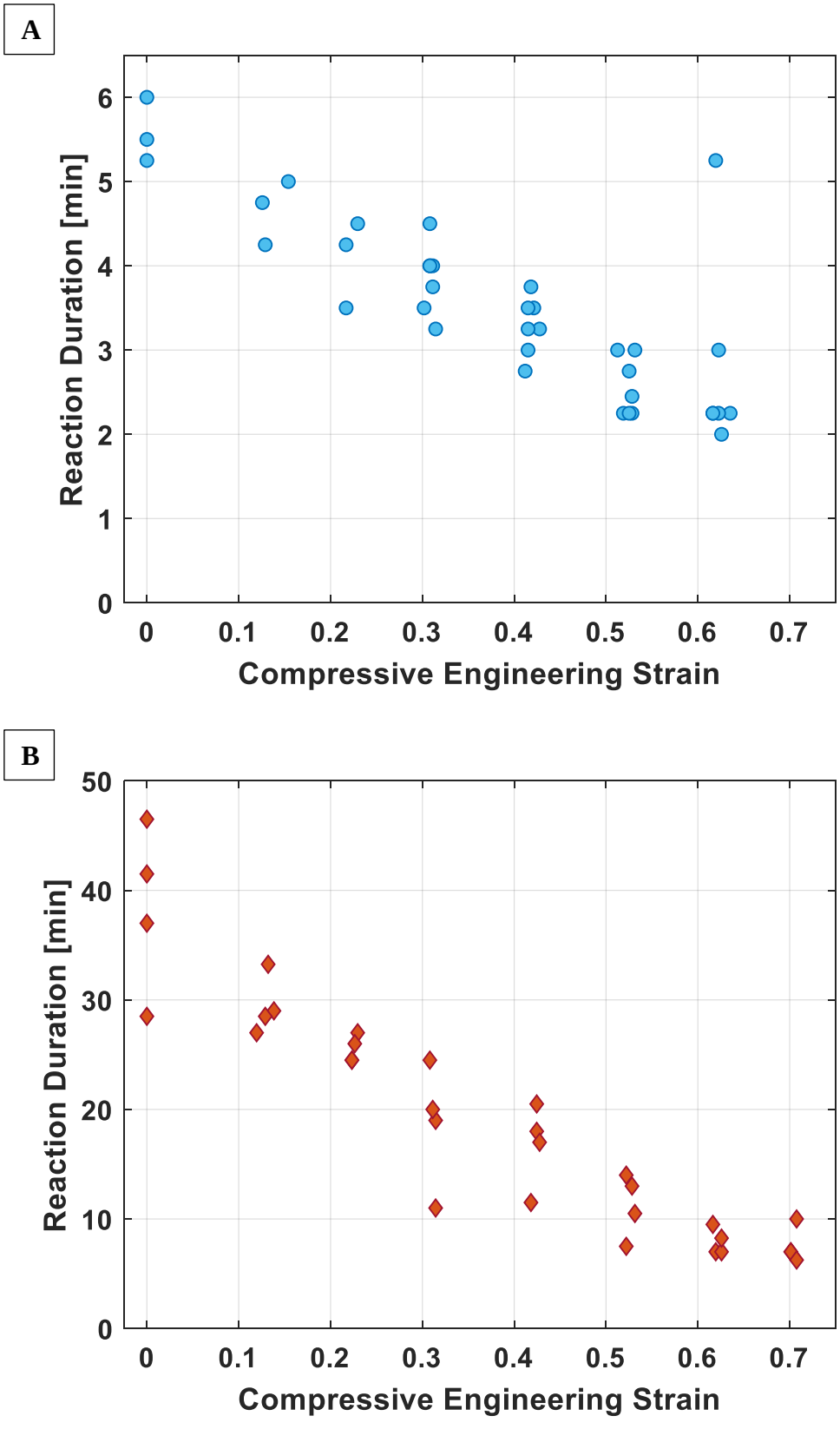

Figure 3-3: Plots of Reaction Duration v Strain for A) DI water and B) caffeine-doped seawater

These reactions were also timed, and results are shown in Figure 3-3. Measurement error was ±0.25 minutes for Duration and ±0.00314 in Strain. Results show a dramatic relationship between reaction rate and strain. While caffeinated seawater reactions did take longer than DI water reactions, both types of water exhibit a trend of increasing reaction rate for increased strain level. At the extreme end of this trend, high-strain samples in DI water would react so quickly and so violently that the still-reacting aluminum sample would be thrown upwards by the force of the hydrogen bubbling underneath it, temporarily halting the reaction (see Section 2.4, Types of Reactant Water).

The general trends seen in activated-aluminum–water reactions were that strain did not affect the hydrogen production fraction, but high levels of strain did significantly accelerate the reaction. Additional details of these trends are discussed in the following section.

3.2 Evidence of Unreacted Aluminum

As mentioned previously, Figure 3-1A, Hydrogen Yield versus Strain for DI water, shows much more variation in the reactions of higher strain levels (0.3 – 0.6). In all of the instances where a yield fraction less than 0.96 was measured, including all samples at 0.5 and 0.6 strain levels, aluminum filaments were seen in the product slurry (See Figure 3-4A, a variant of Figure 3-1A, marking which measurements produced filaments). These filaments were observed as reflecting bits of metal throughout the AlOOH slurry, on the order of 0.1 mm at most. Figure 3-5A presents an image of the filaments mixed throughout the slurry in the sieve compared to a product slurry without any filaments.

While these filaments did not appear to be reacting when washed with DI water in the sieve, when they were left in a vial containing product slurry, filaments were not observed in the slurry 24 hours later.

Similarly to the aluminum filaments seen in high strain reactions of DI water, the caffeinated seawater reactions occasionally produced aluminum nuggets. Compared to the filaments, these were much larger, on the order of 5 mm. Only one to three nuggets were observed in the products of the reaction samples of 0.1, 0.2, and 0.3 strain. The nuggets were seen producing hydrogen in the sieve when washed with DI water (example presented in Figure 3-5B).

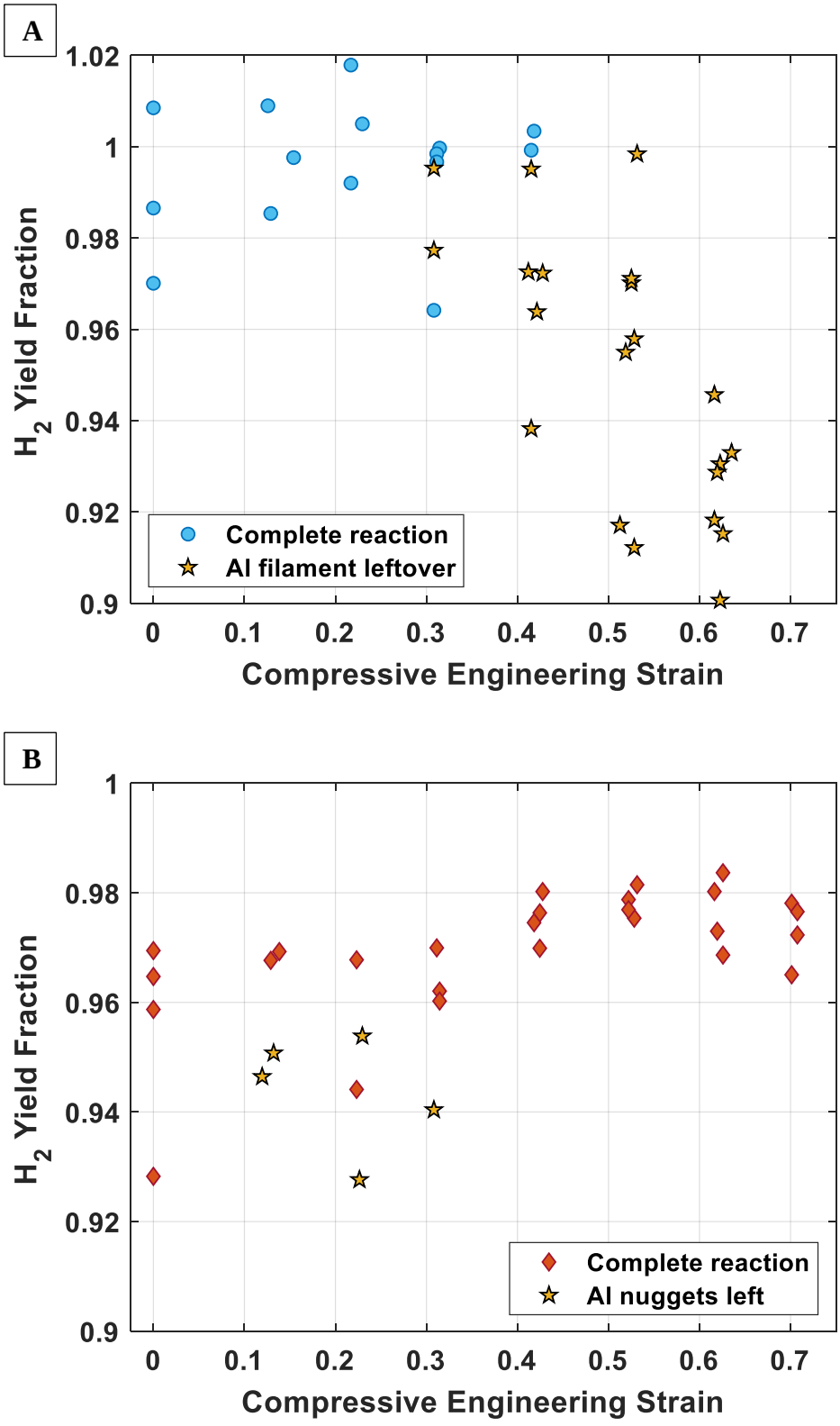

Figure 3-4: A variant of Figure 3-1 where reactions in which aluminum was seen in the product has been marked. A) is from the DI water reaction, and B) is from the caffeinated seawater reaction.

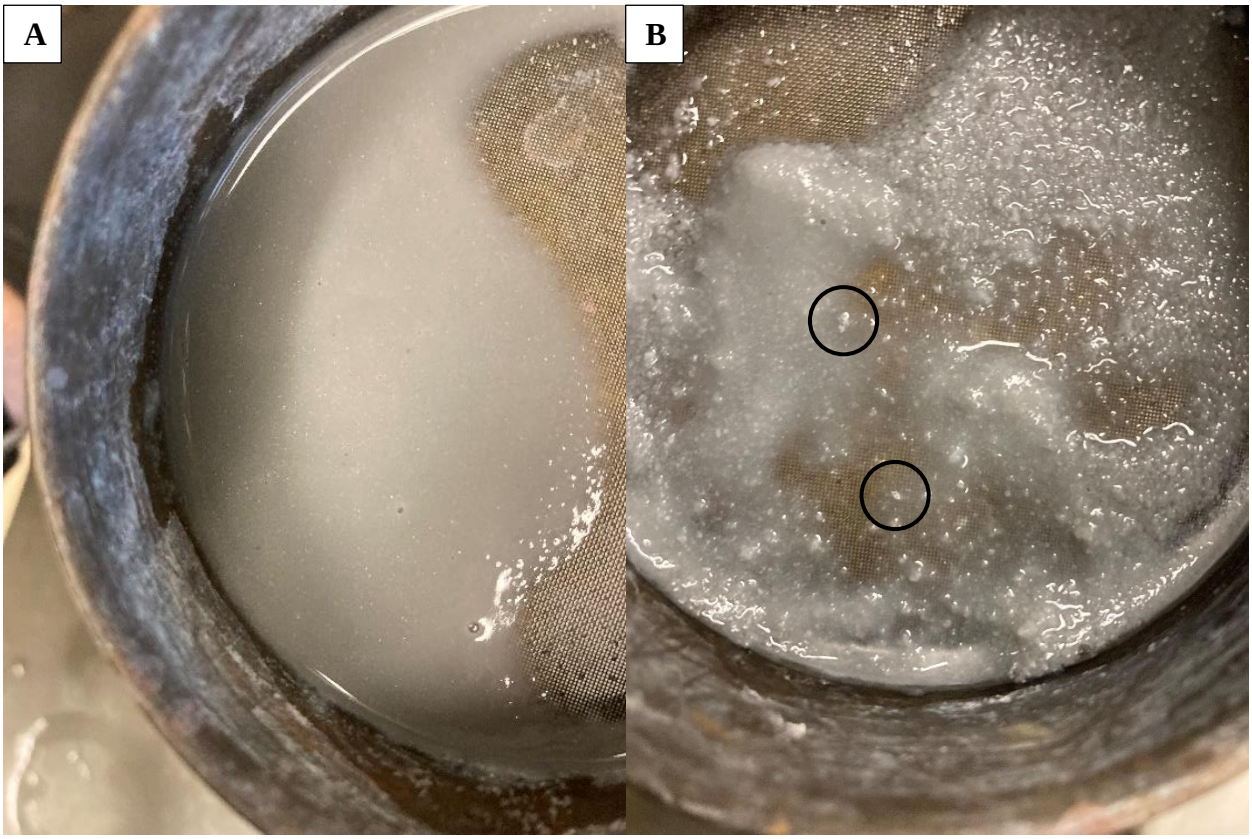

Figure 3-5: A) Aluminum filaments from the DI reaction throughout the product slurry. B) Aluminum nuggets from the caffeine-doped seawater reaction in the product slurry. The nuggets have been circled.

Figure 3-6 shows the same unreacted aluminum data highlighted as Figure 3-4, but as a modification of Figure 3-3 (Duration versus Strain). No general trend was observed after comparing the durations of DI reactions that did or did not produce aluminum filaments. Therefore, the existence or not of aluminum filaments in the product of a reaction is not a consequence of ending a reaction too early. In caffeine-doped seawater reactions, unreacted aluminum reactions appear to be on the shorter side of a relative trend for longer reactions and lower strain levels. Thus, these reactions may have benefited from additional time to fully react, despite no visible hydrogen bubbles emerging from the viscous product slurry at the time. In both cases, further research is required to determine the cause of these filaments and nuggets.

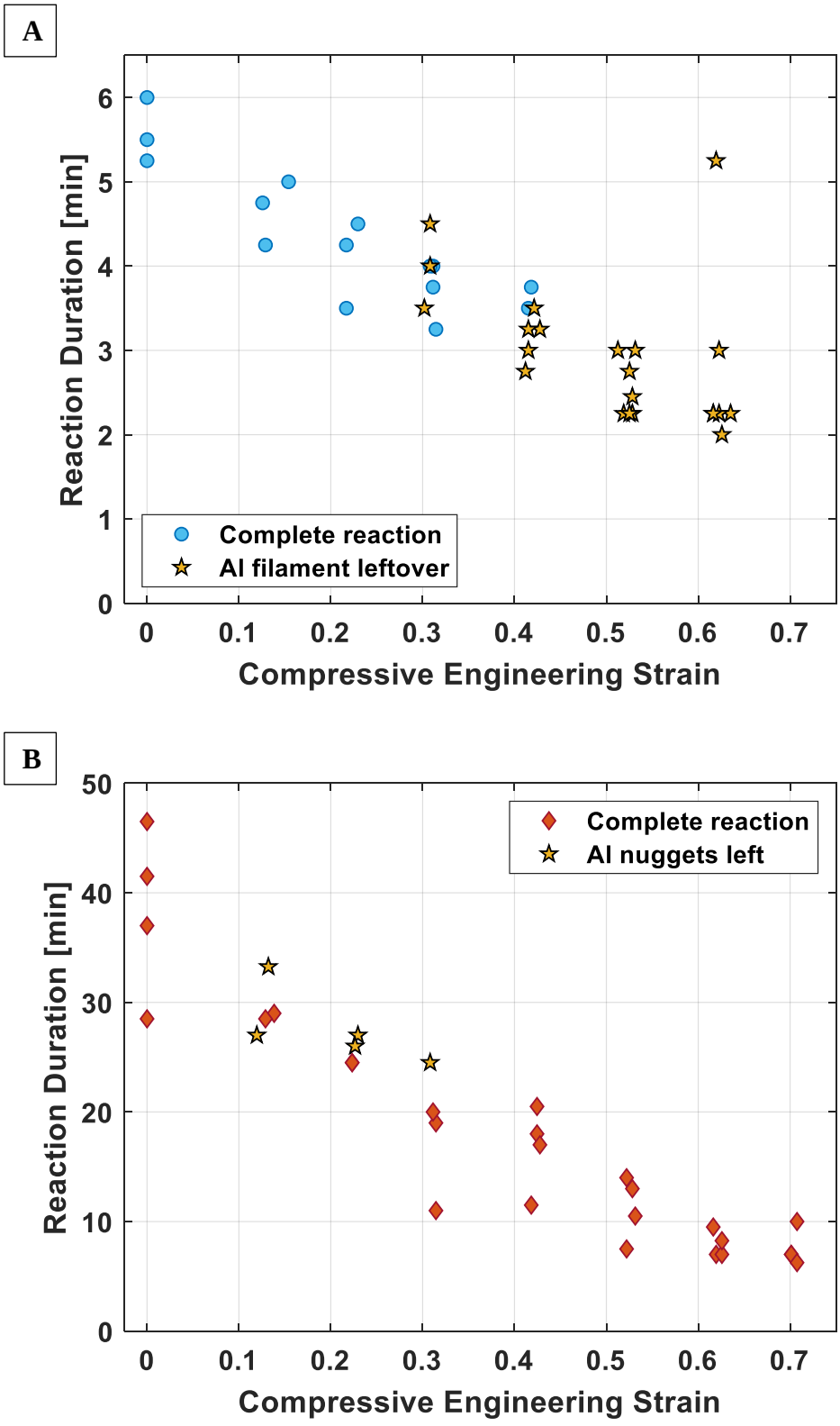

Figure 3-6: A variant of Figure 3-3 where reactions in which aluminum was seen in the product has been marked. A) is from the DI water reaction, and B) is from the caffeinated seawater reaction.

In order to verify that the aluminum filaments seen in the product slurry were, in fact, aluminum, and not a minor alloying element (See Section 2.1,
Cold Working Aluminum for Controlled Strain Levels), SEM/EDS imaging was performed. Elements scanned for included Al, Si, Mn, Fe, Cu, Zn, Ga, and In. Produced images can be seen in Figure 3-7, with an SEM image in the top left and elemental scans in the remaining images. The elemental scans are replications of the same SEM image, but are only colored to reflect when an electron is emitted from the specified element. The image shows a flaky object in its center that appeared similar to the filaments throughout the product slurry and was found to be aluminum. The area around it, which is more cloudy in texture, appears to be AlOOH (as shown in literature [27]), thus the additional hits of aluminum in this region of the aluminum map (top right). The gallium (bottom right) and indium (bottom left) maps show the presence of both in the liquid metal balls sitting on top of the AlOOH slurry and dispersed throughout the slurry itself. Additional maps of Si, Mn, Fe, Cu, and Zn were produced, but none contained significant data as compared to the three elements shown below.

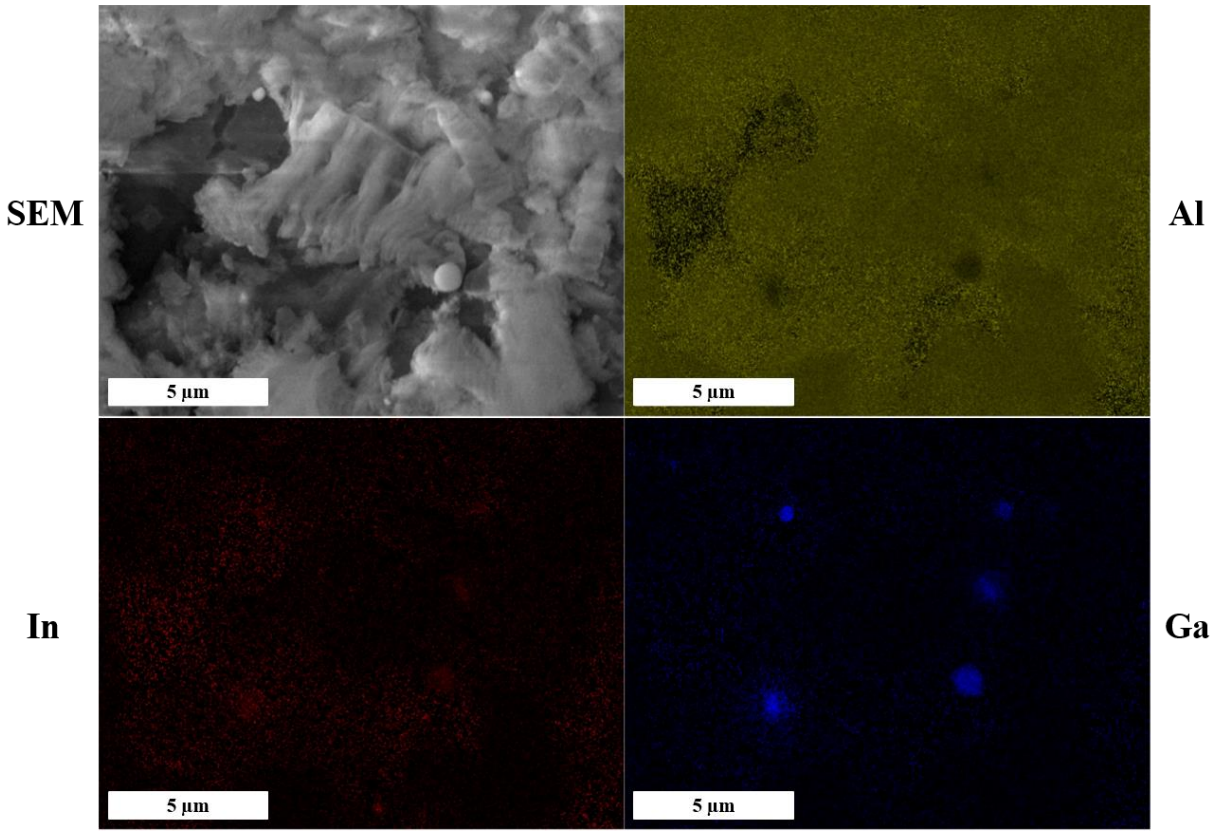

Figure 3-7: SEM/EDS maps of an aluminum filament producing during a DI water reaction

3.3 SEM Comparison

SEM imaging of 0.0 and 0.6 strain samples, both treated-and-reacted and untreated controls, were conducted. Images of the control samples can be seen in Figure 3-8. While the unstrained sample in Figure 3-8A is smooth and polished in the as-received condition, the strained sample in Figure 3-8B has a number of surface features and light breakage.

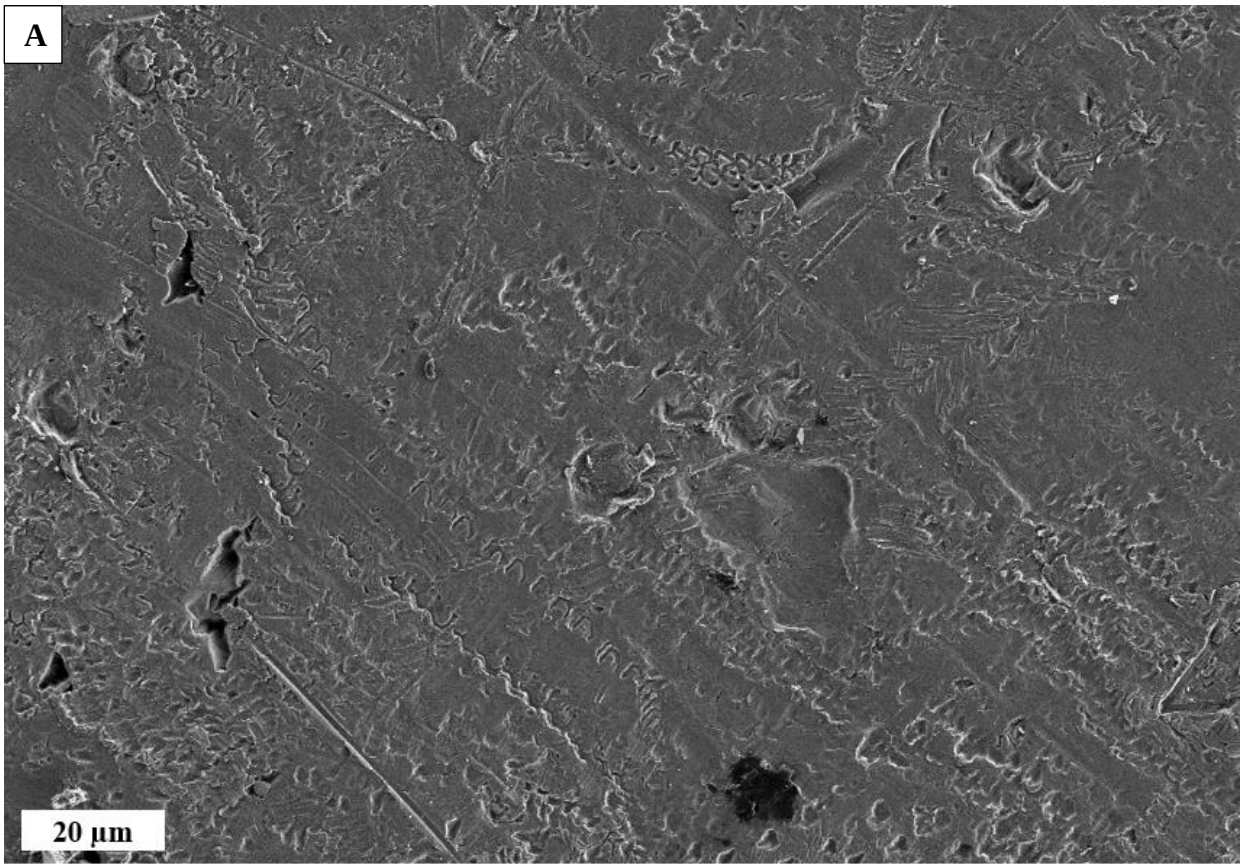

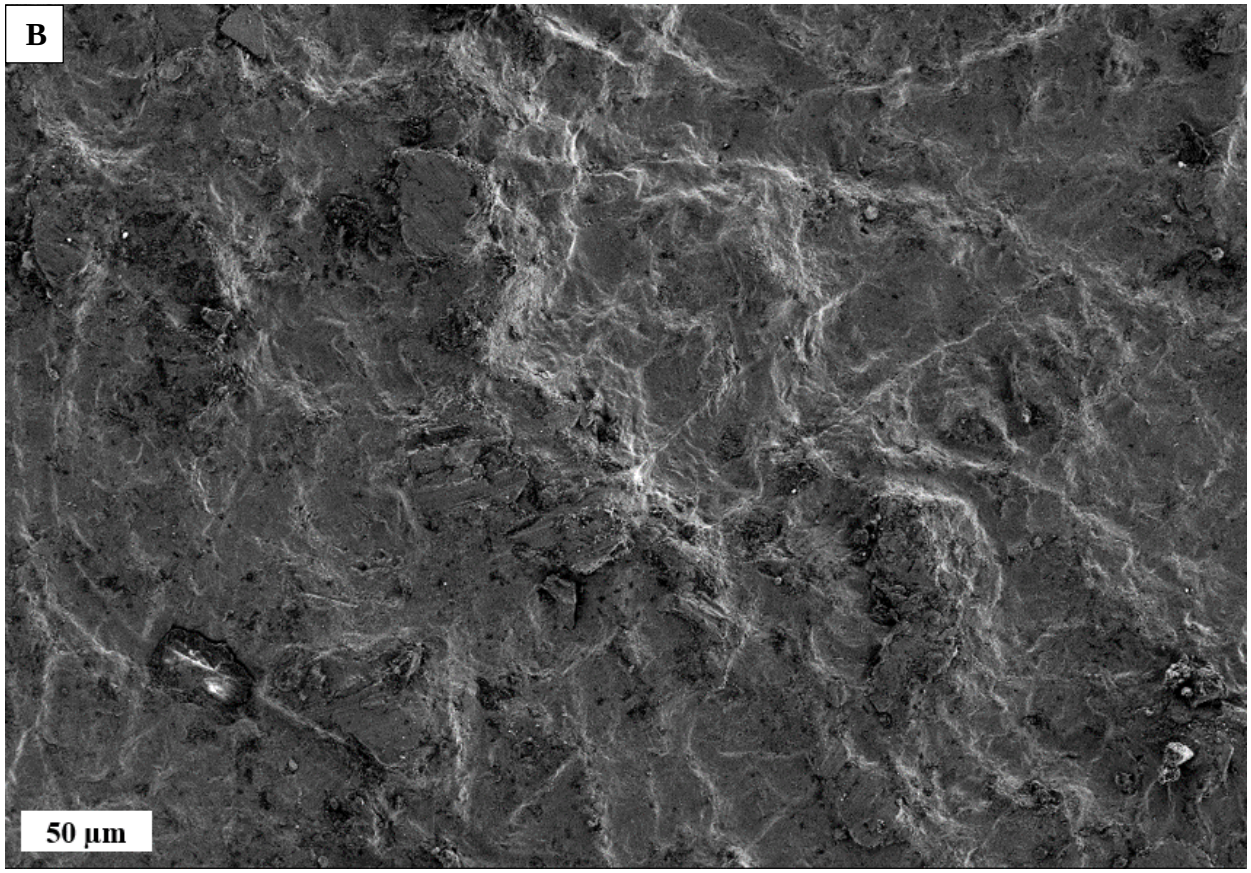

Figure 3-8: SEM images of control samples with A) 0.0 Strain, B) 0.6 Strain

The images of the treated and reacted 0.0 strain sample can be seen below in Figure 3-9. In Figure 3-9A, the top surface of the sample, one of the two originally treated with eGaIn, shows cracking and a circular pattern on the order of 1mm in diameter. This pattern was not seen on the untreated sample. Similar circular patterns were seen across the sample surface but were not visible with the naked eye despite their size. In Figure 3-9B, looking at a side face of the sample, the delamination phenomenon is occurring as seen in published results [27]. This delamination appeared in cracks across the sample in addition to regions of the sample's side surface.

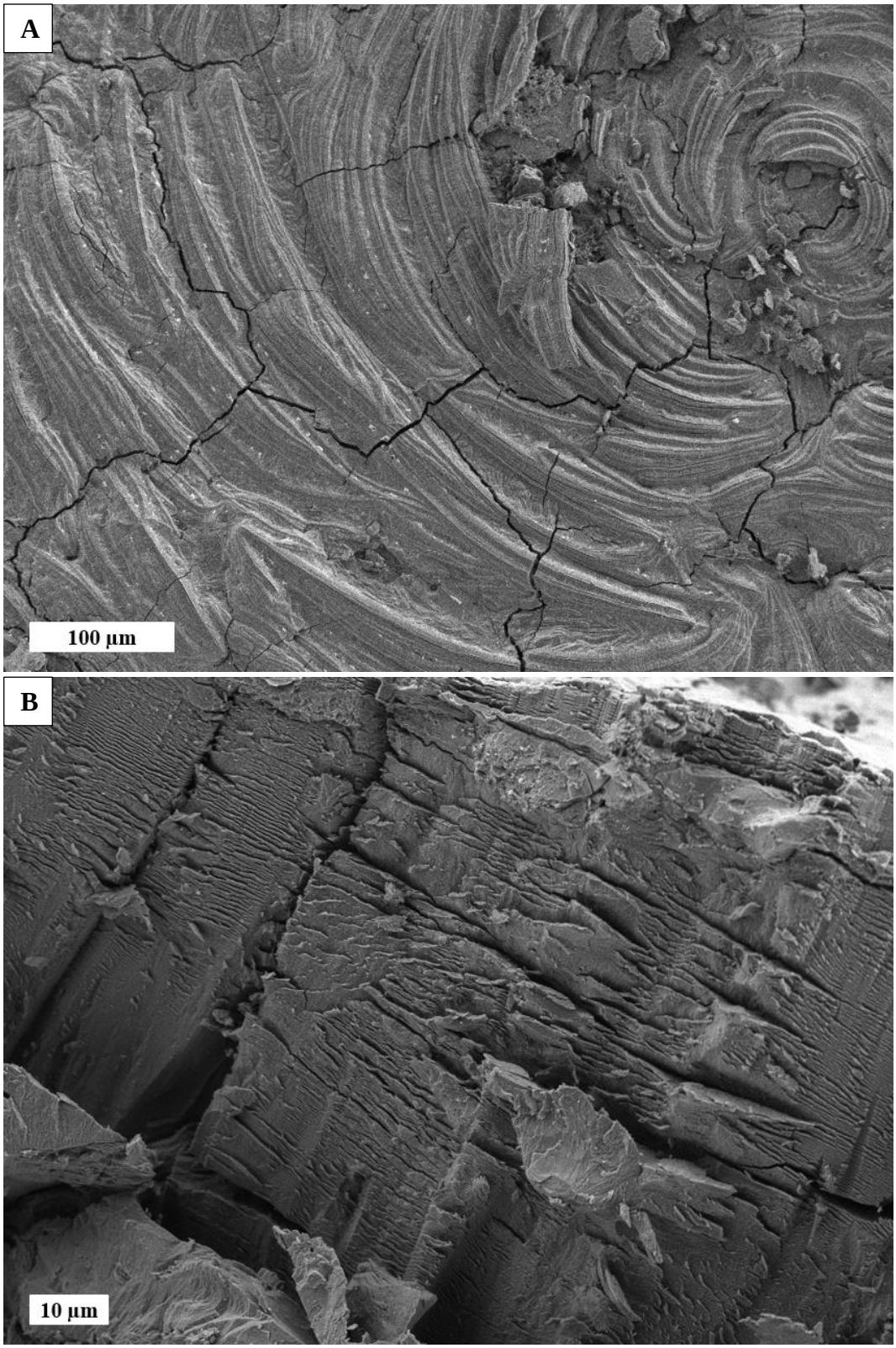

Figure 3-9: SEM images of an unstrained sample that were treated with eGaIn and reacted for three hours in humid air

The images of the 0.6 strain sample are found in Figure 3-10. All these images were taken on the top surface of the sample. In Figure 3-10A, a circular pattern is seen radiating outwards to the image's top left while significant upheaval is seen in the center right and small bulbs are seen around the edges of the image. In Figure 3-10B, a number of circular patterns are seen around cracks in the sample. In Figure 3-10C, highly delaminated grains are seen at the center of an eruption zone.

Compared to Figure 3-9A, the circular patterns seen in Figure 3-10 A and B are on much smaller scales, on the order of tens of micrometers as opposed to millimeters for the unstrained sample. Figure 3-10C is a magnified image of an eruption zone similar to the upheaval region seen in Figure 3-10A. It appears that the bulbs seen around the edges of Figure 3-10A are identical to the highly delaminated grains seen in Figure 3-10C. Thus, it is concluded that highly delaminated grains are erupting out of the sample bulk and causing circular patterns around their eruption zone. It is noted that the ejected grains are likely smaller than the grain sizes in the bulk of the sample, though this is unconfirmed.

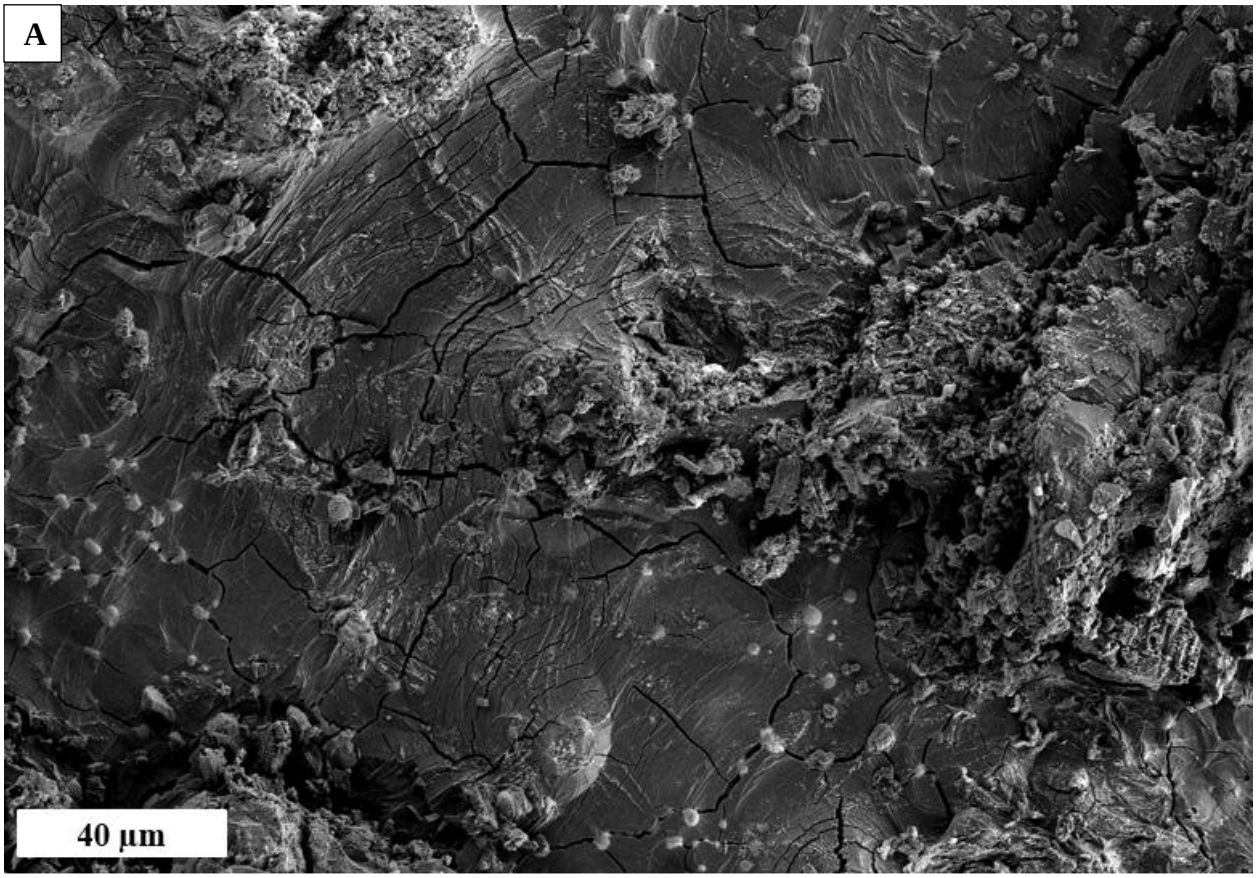

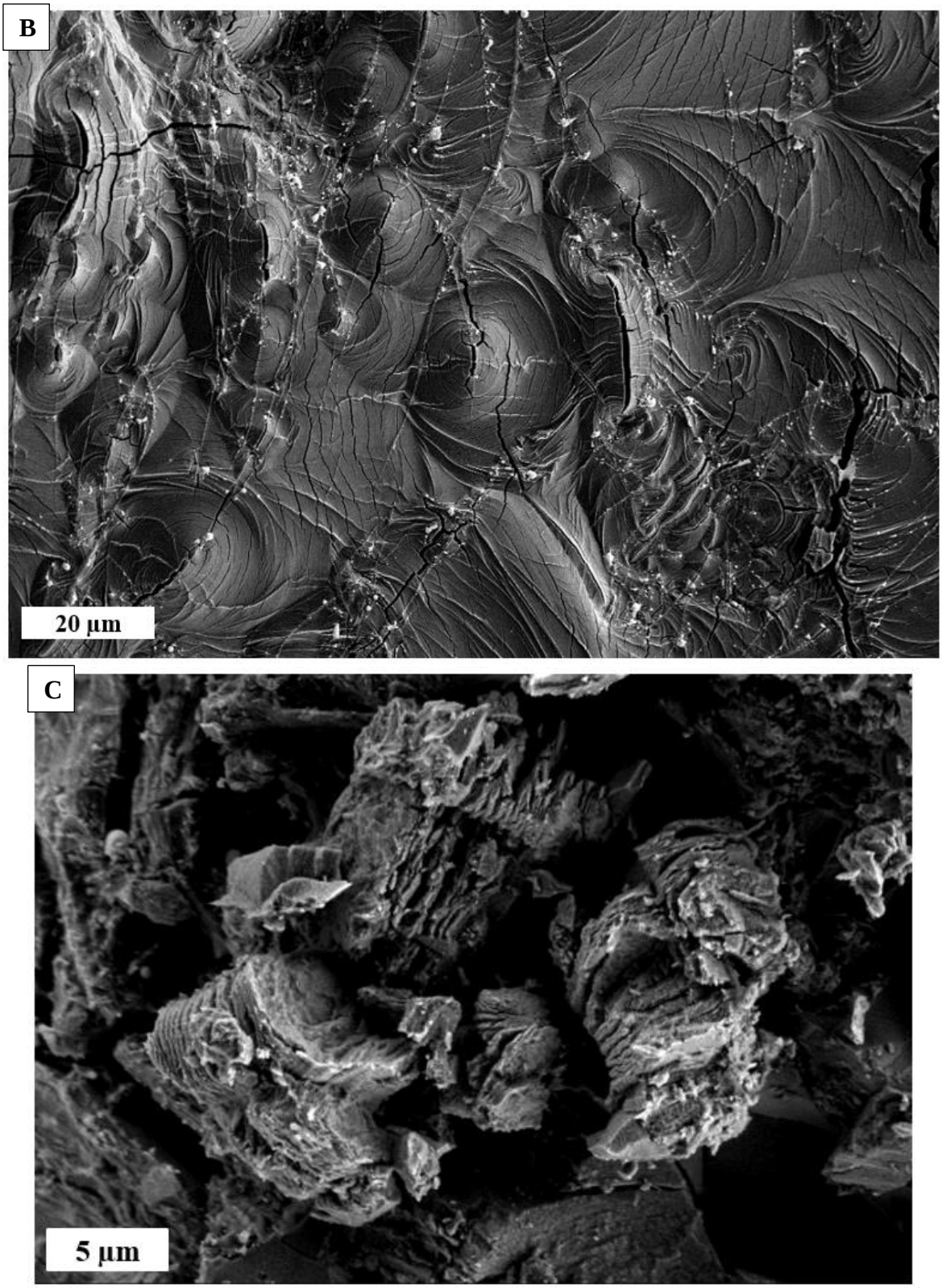

Figure 3-10: SEM images of a highly strained sample that were treated with eGaIn and reacted for one hour in humid air

Regarding the original images from literature of delaminated grains in Figure 1-4 [27], this delamination is occurring in surface cracks, as seen in Figure 3-9B, and in ejected grains, as seen in Figure 3-10C. It appears that the circular patterning is occurring around ejection sites. As the delamination and circular patterning occurred in both the highly strained and unstrained samples, neither seems to be entirely an effect of strain, though the highly strained samples did see both phenomena occur in greater numbers and on a smaller scale, so some relationship is likely. Further work would be necessary to fully understand that relationship.

Chapter 4: Conclusions and Future Work

4.1 Conclusions

This thesis seeks to develop understanding of activated-aluminum–water reactions and how they are affected by strain. While results showed no correlation between strain and the reaction yield, strain did affect the reaction's duration as well as the scale of the micromechanics.

By annealing and cold-rolling 1100 aluminum, strain was created in nearly-pure samples. Samples were then activated by treatment with eGaIn at 120°C for two hours. By testing sample hardness values, this was shown to have minimal impact on the residual stress state.

Samples were reacted in either DI water or caffeine-doped simulated seawater (0.1M caffeine, 0.6M NaCl). Hydrogen yield fraction was reported as experimental moles produced over theoretical moles, as calculated by the ideal gas law from the volume of collected gases and density from the aluminum mass, respectively. Results showed no correlation between hydrogen yield fraction and strain level. Reaction durations were shortened at heightened strain levels.

Reactions at high strain levels (0.3-0.6) in DI water yielded leftover aluminum filaments that appeared to cause variability in hydrogen yield fraction. Similar occurrences in caffeine-doped seawater were observed at lower strain levels, but appeared to be impacted by the duration measurement. The unreacted aluminum filaments were confirmed to be aluminum by SEM/EDS. All unreacted aluminum did react when allowed to remain in the product slurry for 24 hours.

Additional samples at the 0.0 and 0.6 strain levels were imaged in an SEM after beginning to react in humid air. Circular patterns were seen centered around eruption zones where highly delaminated grains were ejected from the sample bulk. These grains and circular patterns occurred in smaller scales and in greater quantities at the higher strain level. Grain delamination was only seen to occur in surface cracks and on the ejected grains.

In summary, this thesis has presented results of experiments with controlled strain levels in near-pure aluminum samples, showing (1) how activated-aluminum–water reactions may be accelerated by residual stresses in the material, (2) how unreacted aluminum may form as an effect of the same, and (3) how stress qualitatively changes the microstructural reaction. While future work is needed to explore these findings in more depth, the general effects of strain are beneficial for activated-aluminum reactor design. The technology of activated aluminum is still in its infancy, but it promises safe energy storage and generation capabilities.

4.2 Future Work

While this thesis furthers the understanding of how aluminum stress states may affect activated-aluminum–water reactions, it poses a number of further questions as to why those effects occur, and how they can be utilized for the benefit of the society.

Unreacted aluminum was seen in a number of reactions, most prominently at high strain levels in DI water reactions. To fully comprehend this phenomenon, precise measurements of a reaction's hydrogen production over time is necessary. Since these aluminum filaments disappeared over the 24 hours immediately following the reaction, it is highly likely that they continue to react and produce hydrogen gas at a slower rate than the rest of the reaction. The total hydrogen production should be compared to data produced in Figure 3-1, where the effect of the unreacted aluminum's disappearance may be related to the variability noticed in this plot. The mechanics of why this occurs require further study as well. An examination of grain sizes and shapes, and dislocation densities, may provide insight as to why they occur.

In SEM imaging, ejected grains were seen at different size scales and in different quantities depending on the strain level of the sample. In both cases, the size and shape of the ejected grains suggests that they are not entire grains from the bulk, so potential future work may explore variations in dislocation densities as a potential source of these ejected grains. It would also be necessary to observe the grain sizes and shapes in the aluminum prior to reaction in order to better comprehend the relative scales of the ejected grains.

Using the trends of strain effects presented in this thesis, potential uses of activated aluminum may be tailored to maximize their usefulness to humanity. Reactor designs may incorporate the understanding of time scales, varied by strain levels, to optimize the speed of the reaction.

Finally, previous and present research efforts into activated aluminum have primarily focused on minimally alloyed metal samples. Practical reactors, however, would be plagued by supply issues if they were designed to rely on pure aluminum alone. Additional work is needed to explore how individual alloying elements, common in processed and scrap aluminum, effect this reaction and its products. With the plethora of aluminum alloys in commercial use, reactor designs should be made to be as flexible as possible with respect to all alloys and types of water used for reaction.

Appendix of Hydrogen Production Data

Measured thickness [mm]	Eng. Strain [εe-1] (Compression Negative)	Mass Al [g]	Mass Eutetic Coated Al [g]	Mass Eutectic [g]	eGaIn wt%	Ambient Temp [°C]	Ambient Pressure [PaE2]	Apparent H2 Yield Volume [L]	Pressure Difference due to Thermal Expansion [0.5 mL]	Duration [min]	Water Vapor Pressure [Pa]	Reaction Yield Exp: Volume H2 [L]	Reaction Yield Fraction
DI Water													
1.22	0.616	0.29654	0.32099	0.02445	0.076	21.0	1009	0.3975	11.0	2.25	2478.1	0.382	0.918
1.82	0.428	0.27761	0.29758	0.01997	0.067	21.0	1009	0.3950	12.5	3.25	2478.1	0.379	0.972
1.55	0.513	0.27614	0.29374	0.01760	0.060	21.1	1009	0.3725	13.0	3.00	2493.4	0.356	0.917
1.50	0.528	0.26467	0.27993	0.01526	0.055	21.0	1018	0.3700	14.0	2.45	2478.1	0.353	0.958
1.20	0.623	0.28842	0.30620	0.01778	0.058	21.0	1018	0.3875	8.5	3.00	2478.1	0.373	0.931
1.21	0.619	0.29775	0.31966	0.02191	0.069	21.1	1018	0.3975	6.0	5.25	2493.4	0.385	0.929
1.49	0.531	0.28211	0.30383	0.02172	0.071	21.1	1018	0.4100	17.0	3.00	2493.4	0.392	0.998
2.20	0.308	0.28573	0.30241	0.01668	0.055	21.8	1010	0.4150	10.5	4.00	2602.8	0.400	0.995
1.86	0.415	0.28205	0.29920	0.01715	0.057	21.6	1010	0.4075	6.5	3.25	2571.1	0.394	0.995
1.51	0.525	0.29760	0.31815	0.02055	0.065	21.7	1010	0.4200	9.0	2.75	2586.9	0.406	0.970
1.16	0.635	0.27745	0.29891	0.02146	0.072	21.6	1010	0.3775	6.5	2.25	2571.1	0.364	0.933
1.53	0.519	0.27986	0.31103	0.03117	0.100	21.7	1010	0.3900	8.0	2.25	2586.9	0.376	0.955
2.22	0.302	0.26992	0.29827	0.02835	0.095	21.8	1010	0.3625	7.0	3.50	2602.8	0.349	0.917
1.86	0.415	0.27692	0.30839	0.03147	0.102	21.7	1010	0.3800	8.5	3.00	2586.9	0.366	0.938
1.19	0.626	0.28071	0.30607	0.02536	0.083	21.7	1010	0.3750	6.5	2.00	2586.9	0.362	0.915
1.84	0.421	0.29445	0.31932	0.02487	0.078	21.7	1010	0.4125	7.5	3.50	2586.9	0.399	0.964
1.20	0.623	0.28007	0.29762	0.01755	0.059	21.6	1009	0.3675	4.0	2.25	2571.1	0.356	0.901
1.50	0.528	0.27614	0.29163	0.01549	0.053	21.6	1009	0.3675	5.0	2.25	2571.1	0.355	0.912
1.22	0.616	0.27923	0.30260	0.02337	0.077	21.3	1007	0.3850	6.0	2.25	2524.2	0.372	0.946
1.51	0.525	0.27924	0.30039	0.02115	0.070	21.4	1007	0.3975	11.0	2.25	2539.8	0.382	0.971
1.87	0.412	0.28410	0.30498	0.02088	0.068	21.5	1007	0.4050	11.5	2.75	2555.4	0.389	0.973
2.20	0.308	0.26705	0.28379	0.01674	0.059	21.5	1006	0.3825	8.0	4.50	2555.4	0.369	0.977
3.18	0.000	0.28859	0.30564	0.01705	0.056	21.3	1008	0.4100	13.0	5.25	2524.2	0.394	0.970
2.18	0.314	0.26217	0.27627	0.01410	0.051	21.0	1009	0.3850	14.0	3.25	2478.1	0.368	1.000
2.77	0.129	0.26880	0.28289	0.01409	0.050	21.1	1009	0.3875	11.0	4.25	2493.4	0.372	0.985
2.49	0.217	0.27025	0.28361	0.01336	0.047	21.0	1009	0.3925	12.5	3.50	2478.1	0.376	0.992
3.18	0.000	0.26966	0.28474	0.01508	0.053	20.8	1018	0.3950	14.5	6.00	2447.7	0.378	1.009
2.69	0.154	0.26148	0.27040	0.00892	0.033	21.0	1018	0.3800	14.0	5.00	2478.1	0.363	0.998
2.45	0.230	0.28681	0.30481	0.01800	0.059	21.0	1018	0.4200	19.5	4.50	2478.1	0.400	1.005
2.19	0.311	0.28602	0.30019	0.01417	0.047	20.8	1018	0.4150	17.5	3.75	2447.7	0.396	0.998
1.86	0.415	0.27203	0.29179	0.01976	0.068	20.9	1018	0.3975	19.5	3.50	2462.9	0.378	0.999
1.85	0.418	0.29707	0.32120	0.02413	0.075	21.2	1018	0.4350	22.0	3.75	2508.8	0.414	1.003
2.19	0.311	0.29908	0.31091	0.01183	0.038	21.2	1018	0.4350	22.0	4.00	2508.8	0.414	0.997
2.49	0.217	0.28091	0.29894	0.01803	0.060	21.2	1018	0.4250	35.0	4.25	2508.8	0.398	1.018
2.78	0.126	0.28025	0.29808	0.01783	0.060	21.1	1018	0.4200	34.0	4.75	2493.4	0.393	1.009
3.18	0.000	0.27767	0.28889	0.01122	0.039	21.1	1018	0.4075	33.0	5.50	2493.4	0.381	0.987
2.20	0.308	0.27892	0.29923	0.02031	0.068	21.6	1009	0.3925	8.0	4.00	2571.1	0.379	0.964

Measured thickness [mm]	Eng. Strain [ee-1] (Compression Negative)	Mass Al [g]	Mass Eutetic Coated Al [g]	Mass Eutectic [g]	eGaIn wt%	Ambient Temp [°C]	Ambient Pressure [PaE2]	Apparent H2 Yield Volume [L]	Pressure Difference due to Thermal Expansion [0.5 mL]	Duration [min]	Water Vapor Pressure [Pa]	Reaction Yield Exp: Volume H2 [L]	Reaction Yield Fraction
Caffeine-Doped Seawater													
2.20	0.308	0.26719	0.29250	0.02531	0.087	21.6	1015	0.3600	-4.0	24.50	2571.1	0.352	0.940
2.45	0.230	0.26902	0.28857	0.01955	0.068	21.9	1016	0.3675	-4.0	27.00	2618.7	0.360	0.954
2.80	0.119	0.27954	0.29402	0.01448	0.049	21.8	1018	0.3775	-4.0	27.00	2602.8	0.370	0.946
2.76	0.132	0.29500	0.31017	0.01517	0.049	21.8	1016	0.4000	-4.0	33.25	2602.8	0.392	0.951
2.46	0.226	0.28156	0.29777	0.01621	0.054	21.9	1006	0.3775	-4.0	26.00	2618.7	0.370	0.928
0.95	0.701	0.26596	0.29934	0.03338	0.112	21.5	1015	0.3750	2.0	7.00	2555.4	0.364	0.978
0.93	0.708	0.28686	0.32043	0.03357	0.105	21.6	1016	0.4000	1.0	10.00	2571.1	0.390	0.972
1.22	0.616	0.29251	0.31491	0.02240	0.071	22.0	1006	0.4150	0.0	9.50	2634.8	0.405	0.980
1.52	0.522	0.27748	0.29893	0.02145	0.072	21.3	999	0.3975	4.0	7.50	2524.2	0.386	0.979
1.21	0.619	0.27834	0.29738	0.01904	0.064	21.2	999	0.3950	1.5	7.00	2508.8	0.384	0.973
2.74	0.138	0.28077	0.29482	0.01405	0.048	21.4	1004	0.3925	-4.0	29.00	2539.8	0.385	0.969
2.47	0.223	0.27825	0.29482	0.01657	0.056	21.5	1003	0.3800	-4.0	24.50	2555.4	0.372	0.944
2.18	0.314	0.27456	0.29482	0.02026	0.069	21.5	1003	0.3825	-3.0	19.00	2555.4	0.374	0.962
1.83	0.425	0.26471	0.28930	0.02459	0.085	21.6	1016	0.3700	-3.0	18.00	2571.1	0.362	0.976
1.49	0.531	0.28096	0.29822	0.01726	0.058	21.3	1015	0.3950	0.0	10.50	2524.2	0.385	0.981
1.19	0.626	0.27945	0.29337	0.01392	0.047	21.4	1015	0.3950	2.0	7.00	2539.8	0.384	0.984
2.19	0.311	0.27852	0.29330	0.01478	0.050	22.0	1026	0.3825	-4.0	20.00	2634.8	0.375	0.970
1.50	0.528	0.26883	0.28735	0.01852	0.064	21.6	1026	0.3725	-1.0	13.00	2571.1	0.363	0.975
3.18	0.000	0.29080	0.30350	0.01270	0.042	21.5	1026	0.3975	-4.0	41.50	2555.4	0.390	0.969
0.95	0.701	0.28315	0.31796	0.03481	0.109	21.8	1017	0.3925	1.5	7.00	2602.8	0.382	0.965
1.82	0.428	0.29404	0.31899	0.02495	0.078	21.7	1017	0.4100	-4.0	17.00	2586.9	0.402	0.980
1.52	0.522	0.27900	0.29738	0.01838	0.062	21.7	1016	0.3900	-2.0	14.00	2586.9	0.381	0.977
1.83	0.425	0.28594	0.30879	0.02285	0.074	21.6	1006	0.4000	-2.5	20.50	2571.1	0.391	0.970
3.18	0.000	0.28560	0.29491	0.00931	0.032	21.3	1003	0.3950	-4.0	28.50	2524.2	0.387	0.959
2.77	0.129	0.27492	0.29401	0.01909	0.065	21.5	1002	0.3850	-4.0	28.50	2555.4	0.377	0.968
2.47	0.223	0.28004	0.29627	0.01623	0.055	21.4	1000	0.3925	-4.0	24.50	2539.8	0.385	0.968
2.18	0.314	0.28726	0.29926	0.01200	0.040	21.3	1000	0.4025	3.0	11.00	2524.2	0.391	0.960
1.85	0.418	0.27314	0.29778	0.02464	0.083	21.3	999	0.3875	-1.0	11.50	2524.2	0.378	0.975
0.93	0.708	0.26599	0.29482	0.02883	0.098	21.2	1000	0.3800	3.0	6.25	2508.8	0.369	0.977
3.18	0.000	0.28049	0.29482	0.01433	0.049	21.0	1003	0.3900	-4.0	37.00	2478.1	0.382	0.965
1.19	0.626	0.28327	0.30527	0.02200	0.072	21.6	1026	0.3900	1.0	8.25	2571.1	0.380	0.969
3.18	0.000	0.25239	0.27018	0.01779	0.066	21.8	1006	0.3400	-4.0	46.50	2602.8	0.332	0.928

For the above tables, measured data is in blue, and calculated values are in the lighter gray.

References

[1] “International Energy Outlook - U.S. Energy Information Administration (EIA)” [Online]. Available: https://www.eia.gov/outlooks/ieo/index.php. [Accessed: 26-Jun-2022].

[2] “Climate Change: Global Temperature | NOAA Climate.Gov” [Online]. Available: https://www.climate.gov/news-features/understanding-climate/climate-change-global-temperature. [Accessed: 26-Jun-2022].

[3] U.S. Global Change Research Program, Wuebbles, D. J., Fahey, D. W., Hibbard, K. A., Dokken, D. J., Stewart, B. C., and Maycock, T. K., 2017, *Climate Science Special Report: Fourth National Climate Assessment, Volume I*, U.S. Global Change Research Program.

[4] Bindoff, N. L., Cheung, W. W. L., Kairo, J. G., Arístegui, J., Guinder, V. A., Hallberg, R., Hilmi, N., Jiao, N., O’Donoghue, S., Suga, T., Acar, S., Alava, J. J., Allison, E., Arbic, B., Bambridge, T., Boyd, P. W., Bruggeman, J., Butenschön, M., Chávez, F. P., Cheng, L., Cinar, M., Costa, D., Defeo, O., Djoundourian, S., Domingues, C., Eddy, T., Endres, S., Fox, A., Free, C., Frölicher, T., Gattuso, J.-P., Gerber, G., Hallegraef, G., Harrison, M., Hennige, S., Hindell, M., Hogg, A., Ito, T., Kenny, T.-A., Kroeker, K., Kwiatkowski, L., Lam, V. W. Y., Laüfkotter, C., LeBillon, P., Bris, N. L., Lotze, H., MacKinnon, J., de Marffy-Mantuano, A., Martel, P., Molinos, J. G., Moseman-Valtierra, S., Motau, A., Mulsow, S., Mutombo, K., Oyinlola, M., Poloczanska, E. S., Pascal, N., Philip, M., Purkey, S., Rathore, S., Rebelo, X., Reygondeau, G., Rice, J., Richardson, A., Riebesell, U., Roach, C., Rocklöv, J., Roberts, M., Sloyan, B., Smith, M., Shurety, A., Wabnitz, C., and Whalen, C., “Changing Ocean, Marine Ecosystems, and Dependent Communities,” Marine Ecosystems, p. 142.

[5] “Hydrogen and Fuel Cell Technologies Office Multi-Year Research, Development, and Demonstration Plan,” Energy.gov [Online]. Available: https://www.energy.gov/eere/fuelcells/articles/hydrogen-and-fuel-cell-technologies-office-multi-year-research-development. [Accessed: 26-Jun-2022].

[6] 2022, “Energy Density,” Wikipedia.

[7] “Heat Values of Various Fuels - World Nuclear Association” [Online]. Available: https://world-nuclear.org/information-library/facts-and-figures/heat-values-of-various-fuels.aspx. [Accessed: 27-Jun-2022].

[8] “Production of Hydrogen - U.S. Energy Information Administration (EIA)” [Online]. Available: https://www.eia.gov/energyexplained/hydrogen/production-of-hydrogen.php. [Accessed: 27-Jun-2022].

[9] Thomas, G., 2000, “Overview of Storage Development DOE Hydrogen Program,” Natural Gas., p. 14.

[10] Møller, K. T., Jensen, T. R., Akiba, E., and Li, H., 2017, “Hydrogen - A Sustainable Energy Carrier,” Progress in Natural Science: Materials International, **27**(1), pp. 34–40.

[11]"Hydrogen Storage," Energy.gov [Online]. Available: https://www.energy.gov/eere/fuelcells/hydrogen-storage. [Accessed: 27-Jun-2022].

[12]Züttel, A., 2004, "Hydrogen Storage Methods," Naturwissenschaften, **91**(4), pp. 157–172.

[13]Slocum, J. T., 2017, "Characterization and Science of an Aluminum Fuel Treatment Process," Thesis, Massachusetts Institute of Technology.

[14]Khanna, A. S., 2005, "High Temperature Oxidation," *Handbook of Environmental Degradation of Materials*, William Andrew Publishing, Norwich, NY, p. 598.

[15]Goldschmidt, H., 1897, "Method of Producing Metals and Alloys."

[16]Sundaram, D. S., Yang, V., and Zarko, V. E., 2015, "Combustion of Nano Aluminum Particles (Review)," Combust Explos Shock Waves, **51**(2), pp. 173–196.

[17]WONG, S. C., and TURNS, S. R., 1987, "Ignition of Aluminum Slurry Droplets," Combustion Science and Technology, **52**(4–6), pp. 221–242.

[18]Liu, H., Yang, F., Yang, B., Zhang, Q., Chai, Y., and Wang, N., 2018, "Rapid Hydrogen Generation through Aluminum-Water Reaction in Alkali Solution," Catalysis Today, **318**, pp. 52–58.

[19]Belitskus, D., 1970, "Reaction of Aluminum with Sodium Hydroxide Solution as a Source of Hydrogen," J. Electrochem. Soc., **117**(8), p. 1097.

[20]Stanford, K., 2016, "Red Mud – Addressing the Problem," Aluminium Insider [Online]. Available: https://aluminiuminsider.com/red-mud-addressing-the-problem/. [Accessed: 27-Jun-2022].

[21]Razavi-Tousi, S. S., and Szpunar, J. A., 2016, "Effect of Addition of Water-Soluble Salts on the Hydrogen Generation of Aluminum in Reaction with Hot Water," Journal of Alloys and Compounds, **679**, pp. 364–374.

[22]Alinejad, B., and Mahmoodi, K., 2009, "A Novel Method for Generating Hydrogen by Hydrolysis of Highly Activated Aluminum Nanoparticles in Pure Water," International Journal of Hydrogen Energy, **34**(19), pp. 7934–7938.

[23]Kravchenko, O. V., Semenenko, K. N., Bulychev, B. M., and Kalmykov, K. B., 2005, "Activation of Aluminum Metal and Its Reaction with Water," Journal of Alloys and Compounds, **397**(1), pp. 58–62.

[24]Yang, W., Zhang, T., Zhou, J., Shi, W., Liu, J., and Cen, K., 2015, "Experimental Study on the Effect of Low Melting Point Metal Additives on Hydrogen Production in the Aluminum–Water Reaction," Energy, **88**, pp. 537–543.

[25]Hatoum, N., 2013, "Method for Production of Power from Aluminum."

[26]Fischman, J. Z., 2019, "The Development and Characterization of Aluminum Fueled Power Systems and a Liquid Aluminum Fuel," Thesis, Massachusetts Institute of Technology.

[27]Godart, P. T., 2021, "Mechanisms of Liquid-Metal-Activated Aluminum-Water Reactions and Their Application," Thesis, Massachusetts Institute of Technology.

[28]Anderson, T. J., and Ansara, I., 1991, "The Ga-In (Gallium-Indium) System," JPE, **12**(1), pp. 64–72.

[29]HARWOOD, J. J., 1950, "The Influence of Stress on Corrosion (Part 1 of Two Parts)," Corrosion, **6**(8), pp. 249–259.

[30]"McMaster-Carr" [Online]. Available: https://www.mcmaster.com/. [Accessed: 29-Jun-2022].

[31]1991, *ASM Handbook, Vol 2: Properties and Selection: Nonferrous Alloy and Special-Purpose Materials*, ASM International.

[32]1991, *ASM Handbook, Vol 4: Heat Treating*, ASM International.

[33]"Water," NIST Chemistry WebBook, SRD 69 [Online]. Available: https://webbook.nist.gov/cgi/cbook.cgi?ID=C7732185&Mask=4&Type=ANTOINE&Plot=on. [Accessed: 01-Jul-2022].